Electronic Supplementary Material (ESI) for Chemical Science.
This journal is © The Royal Society of Chemistry 2022

Supplementary Information

Intact living-cell electrolaunching ionization mass spectrometry for single-cell metabolomics

Yunlong Shao,[a] Yingyan Zhou,[a] Yuanxing Liu,[a] Wenmei Zhang,[a] Guizhen Zhu,[a] Yaoyao Zhao,*[a] Qi Zhang,[a] Huan Yao,[b] Hansen Zhao,[b] Guangsheng Guo,[a,c] Sichun Zhang,[b] Xinrong Zhang,[b] Xiayan Wang,*[a]

a Center of Excellence for Environmental Safety and Biological Effects, Beijing Key Laboratory for Green Catalysis and Separation, Department of Chemistry and Biology, Beijing University of Technology, Beijing 100124, P. R. China
b Department of Chemistry, Tsinghua University, Beijing 100084, P. R. China
c Minzu University of China, Beijing 100081, P. R. China

***Corresponding authors:**

E-mail addresses: zhaoyaoyao@bjut.edu.cn (Y. Y. Zhao), xiayanwang@bjut.edu.cn (X. Y. Wang)

Contents

1. Experimental Section

Cell lines, reagents and materials. A549, HEK-293, KB, B104, and CPXTNA-2 cells were obtained from the Cell Resource Center of the Institute of Basic Medical Sciences, Chinese Academy of Medical Sciences. Dulbecco's modified Eagle medium (DMEM), trypsin-ethylenediaminetetraacetic acid (0.25%, trypsin-EDTA), penicillin-streptomycin (100 $U \cdot mL^{-1}$), dimethyl sulfoxide (99.5%, DMSO), fetal bovine serum (FBS), and phosphate-buffered saline (PBS) were purchased from Thermo Fisher Gibco. DNase I and collagenase D were purchased from R&D Novus Tocris MerckMillipore Inc. ACK lysis buffer was purchased from Gen-View Scientific Inc. DiO [DiOC18(3), a green fluorescent probe for the cell membrane] was purchased from Shanghai Yesen Biotechnology Co. Ltd. Liposomes were donated by FluidicLab (https://www.fluidiclab.com/). All other reagents were purchased from Thermo Fisher Scientific. Fused silica capillaries were purchased from Yongnian Ruifeng Chromatographic Device Co. The Minute™ plasma membrane protein isolation kit SM-005 was acquired from Invent Biotechnologies, Inc. The long-distance microscope objective lens (50×, 0.42 NA) was manufactured by Mitutoyo. The high-performance, high-speed camera (MEMRECAM ACS-3) was manufactured by NAC Image Technology Inc.

Fabrication of narrow-bore capillaries. A 30-cm-long capillary was cut, and one end was etched using the wet etching protocols established previously by our research group to obtain a tip [1,2]. Then, the capillary tip was stored in an airtight, dust-free environment for future use.

Preparation of cell suspensions. Cells were trypsinized using trypsin-EDTA (0.25%) when grown to a coverage of 80–90%. The trypsinization process was terminated using a fresh culture medium. Then, the trypsin-EDTA-containing residual culture medium was removed by centrifugation (1200 rpm, 3 min), and the obtained cells were resuspended in a DMEM culture medium. Appropriate volumes of cell suspensions were centrifuged at 1200 rpm for 3 min to remove the culture medium and cleaned with 150 mmol/L ammonium formate (pH = 7.4). Finally, the cells were resuspended in 40 mmol/L ammonium formate aqueous solution.

Build an online ILCEI-MS visualization platform. The platform comprised a self-designed and self-manufactured MS ion source and a microscopic high-speed camera system composed of a long-distance microscope objective lens (50×, 0.42 NA) X and a high-performance, high-speed camera (MEMRECAM ACS-3). The operation of the ILCEI-MS system was visually recorded using this platform.

Numerical simulation of hydrodynamics in cell motion process at the exit of the narrow capillary emitter with a constant-inner-diameter

（1）Model settings. To simulate the flow of particles in a multiphase system flow, the Eulerian model was used along with the dynamic mesh method for the dynamic simulation of particle motion. A velocity distribution diagram of the particle at the exit of the emitter was obtained. The Dynamic Mesh Zones software was used for the calculation.

（2）**Border conditions.** The liquid phase system is comprised of water. The flow rate was 1 μL/min, and the I.D.s of the emitters were 16, 50, and 100 μm. At the pressure exit, a 15-μm-diameter rigid particle with a density of 1552 kg/m^3, the same as the cell density, was present. No voltage was applied to the simulation system. Opening the gravity tab and a comprehensive motion trajectory was obtained. The changes in the cell's exit velocity and shear stress received on the cell surface were simulated by computer with increasing capillary diameter.

Verification of cell integrity using DiO. A549 cells in the logarithmic growth phase were collected, the medium was removed, and the cells were rinsed with PBS 3 times. A total of 5 mL of 10 μmol/L DiO working solution (dissolved in DMEM supplemented with 10% FBS) was added to the culture flask, which was then incubated at 37°C for 15 min, rinsed with PBS 3 times, and trypsinized to prepare a cell suspension. These cells were injected using ILCEI-MS and collected at the ion inlet of the mass spectrometer. Then, their morphology was characterized by a microscopic imaging method.

Verification of cell viability using CCK8. A549 cells were selected after subculture for 2 days for the experiment. A549 cells that passed the ILCEI-MS sampling device in front of the ion inlet of the mass spectrometer were selected as the experimental group (using a centrifuge tube containing culture medium to receive the cells). The cells that had undergone the ILCEI-MS sample preparation process were collected as the control group (the cells were immediately centrifuged and resuspended in the medium after the sample preparation process was completed), and the cells without any treatment were used as the blank group. Next, 5000 cells/well were inoculated on a 96-well culture plate. Each sample was prepared with triplicate wells, to which 10 μL of the CCK8 reaction solution was directly added after inoculation, and the cells were incubated for 30 min at 37 °C in the dark. A microplate reader (SpectraMax M4, AD, USA) was used to measure the absorbance at a wavelength of 450 nm.

Preparation of cell lysis solution. The cell suspension (1 mL) with a density of 1×10^7 cells/mL was centrifuged at 1000 rpm for 5 min at room temperature. After the supernatant was removed, the cells were resuspended in 200 μL of 80% (v/v) methanol aqueous solution at -80°C and sonicated in an ice bath for 5 min. After incubating at -20°C for 30 min, the solution was sonicated in an ice bath for 5 min, followed by centrifugation for 20 min (4°C, 17,000 g). Finally, the supernatant was taken for MS detection.

Establishment of mouse tumor-bearing models of metastatic lung cancer. A single-cell suspension with a density of 1×10^7 cells/mL was prepared after the A549 cell culture. Nine C57/BL6 male mice aged 6–8 weeks were randomly divided into an experimental group (five mice) and a control group (four mice). The mice were fixed in a mouse fixator, and the tails were wiped with a 75% alcohol cotton ball to disinfect and dilate the blood vessels; the experimental group and the control group were injected with 0.10 mL cell suspension and physiological saline, respectively. The flow rate was controlled during cell injection to prevent embolism. Mouse rearing and experiments were carried out in an SPF laboratory animal room for 20 days.

Preparation of single-cell suspension of mouse tissues. Preparation of Liberase/DNase digestive

solution: The required amount of digestive solution was prepared according to the ratio of 965 μL of 1640 basal medium, 25 μL of 40× collagenase D and 10 μL of 100× DNase I per mL. Mice were killed by cervical dislocation, and their lung, liver and heart organs were harvested. Digestive juice was injected into the tissues by the perfusion method. The tissues were then completely immersed in digestive juice and incubated at 37°C for 30–45 min. The tissue was placed on a 40 μm filter and gently ground to isolate as many tissue cells as possible. The cells were rinsed several times with PBS/EDTA solution until all isolated cells were collected. After centrifugation at 1000 rpm for 5 min, the supernatant was discarded. ACK lysis buffer was added to the cell precipitate at a volume 3-5 times that of the cells, and the cells were gently resuspended. The red blood cells were lysed at room temperature for 2–3 min and centrifuged at 1000 rpm for 5 min, and the supernatant was removed. The appropriate amount of PBS was used to wash the cells twice, and the cells were detected using ILCEI-MS.

It should be noted that to prevent residual cell clumps in the cell suspension from affecting the detection; the cells were filtered again with a 40 μm filter before mass spectrometric detection.

We complied with all relevant ethical regulations, and the animal experiment was approved by the Ethics Committee of Beijing University of Technology, China. The approval number is HS202103001.

Quality control during single-cell detection. (1) We tested a blank sample (cell-free mobile phase) under the same experimental conditions before each cell sample test. Quality control of the detection system was achieved by controlling the intensity and stability of the ion signal in the blank sample, which was seen as the background and was subtracted from the cell detection data during subsequent data processing. (2) We decrease the cell density in the injection capillary by reducing the cell density in the cell suspension; In addition, we use the narrow capillary (the I.D. was slightly smaller than the cell's diameter) for single-cell separation and injection. Due to the confinement effect of narrow inner diameter capillaries, single-cells were adequately isolated with the expanded distance between single-cells in the injection capillary. Finally, we achieved suitable injection flow rates by controlling the injection pressure. Through the above three points, the time interval between single-cells involved in ionization was optimized, which ensured that multiple cell ionization does not occur within one scan time of the mass spectrometer. In order to further improve the controllability of the experiments, we constructed the ILCEI-MS on-line visualization platform, via a large number of on-line visualization characterization data to prove that the electro-launching images of multiple single-cells match the detection signals of mass spectrometry. Based on the above efforts, it is basically guaranteed that each signal peak in total ion chromatogram (TIC) from the ILCEI-MS system corresponds to a single-cell; they are not produced by the superposition of signals from multiple cells.

Single-cell mass spectrometry. All mass spectral data were acquired on an LTQ Orbitrap XL mass spectrometer (Thermo Scientific, San Jose, CA, USA). The MS parameters were set as follows: The voltage was controlled at ~1.4 kV, and the spray current was controlled at 0.2–0.7 μA**,** although slight differences were observed according to specific experimental conditions. The following conditions were used: inlet temperature, 350 °C; resolution, 30000; maximum injection time, 50 ms; AGC target, 1×10^5; and scanning range, *m/z* 100–1000 or 300–1000. The MS-ddMS^2 parameters were set as follows: voltage, 2.3 kV; ion inlet temperature, 350°C; resolution, 30000;

maximum injection time, 500 ms; AGC target, 2×10^5; and scanning range, *m/z* 100–1000. In vitro cultured cells were analyzed using 15 μm inner diameter (I.D.) capillaries. The single-cells obtained from the liver and heart were larger in volume through microscopic observation, therefore, in this part of the experiment, a 25 μm I.D. capillary was used to complete the separation, transport and electroemission ionization mass spectrometry detection of the single-cells.

Data analysis and metabolite identification. A single-cell signal peak must be selected with an intensity greater than 10% of the median intensity of the top 30 peaks in the TIC. Raw data processing was performed on a metabolite data analysis platform developed by our group [3]. The source code of the MATLAB software used is https://github.com/HansenZhao/PeakPicker. The S/N ratio calculation method of single-cell peaks in TIC of ILCEI-MS that refers to the Wei's work [4]. The S/N ratio of single-cell peaks to evaluate the detection sensitivity of ILCEI-MS. Ions of mass spectra with an S/N ratio of >5 and an occurrence frequency of >10% in all cell events were considered as detected signals. Lipid metabolites are the major constituents of cell membranes, and hence, they could be used as a reliable reference for the differentiation of cell profiles and the electrolaunching ionization of sensitive substances. Nonlinear reduction of complex metabolic data sets using a machine learning method is based on t-SNE, which can qualitatively discriminate subtle groups and visualize the difference in the two-dimensional plane. A scatter plot displays the statistics of the difference in the content of a certain metabolite in all the single-cells among each group of samples.

Single-cell metabolites were identified by matching $ddMS^2$ spectra obtained from population cells with the standard spectra using mzCloud (https://www.mzcloud.org/), Human Metabolome Database 5.0 (HMDB) (http://www.hmdb.ca/) and MassBank Database 2.1.8 (http://www.massbank.jp/Index). More information about single-cell metabolite matching could be obtained by referring to various databases available online, including the Kyoto Encyclopedia of Genes and Genomes (KEGG) (https://www.genome.jp/kegg/). Metabolic pathway analysis was performed on MetaboAnalyst 5.0 (http://www.metaboanalyst.ca/).

2. Supplementary Figures

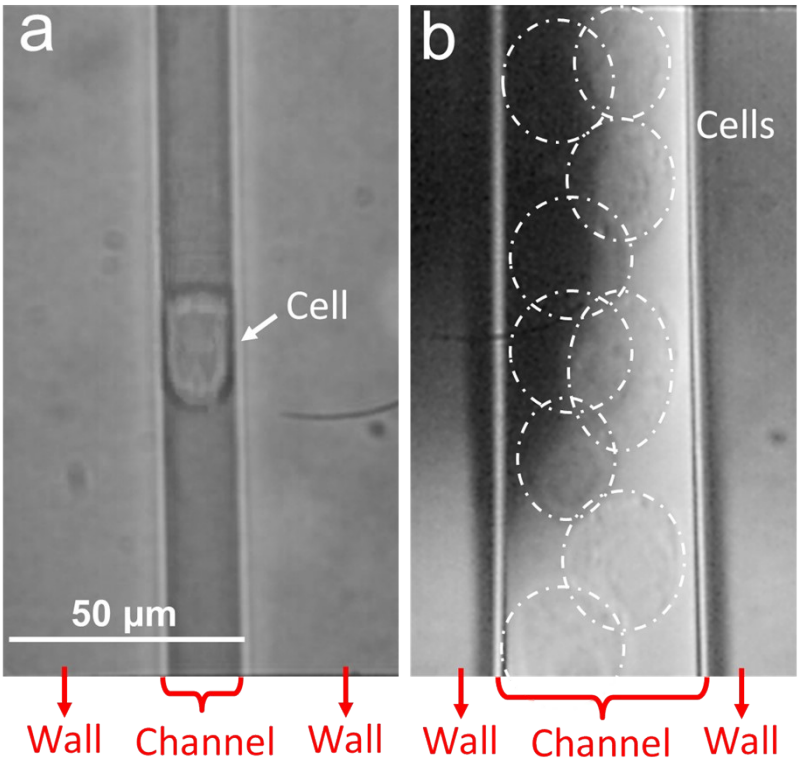

Figure S1. Comparison of single-cell separation effects with different I.D.. (a) 16 μm I.D. capillary, (b) 50 μm I.D. capillary.

Observations on the transport of cell suspensions (A549 cells, diameter ~20 μm) in capillaries with different I.D.s show that single intact cells exist independently and are separated completely in a 16 μm I.D. capillary, whereas obvious cell stacking occurs in a 50 μm I.D. capillary, leading to poor separation. This is due to the more obvious spatial confinement of the narrow-bore capillary. These results suggest that a narrow capillary with an I.D. close to the diameter of a cell is a prerequisite for the separation of single-cells.

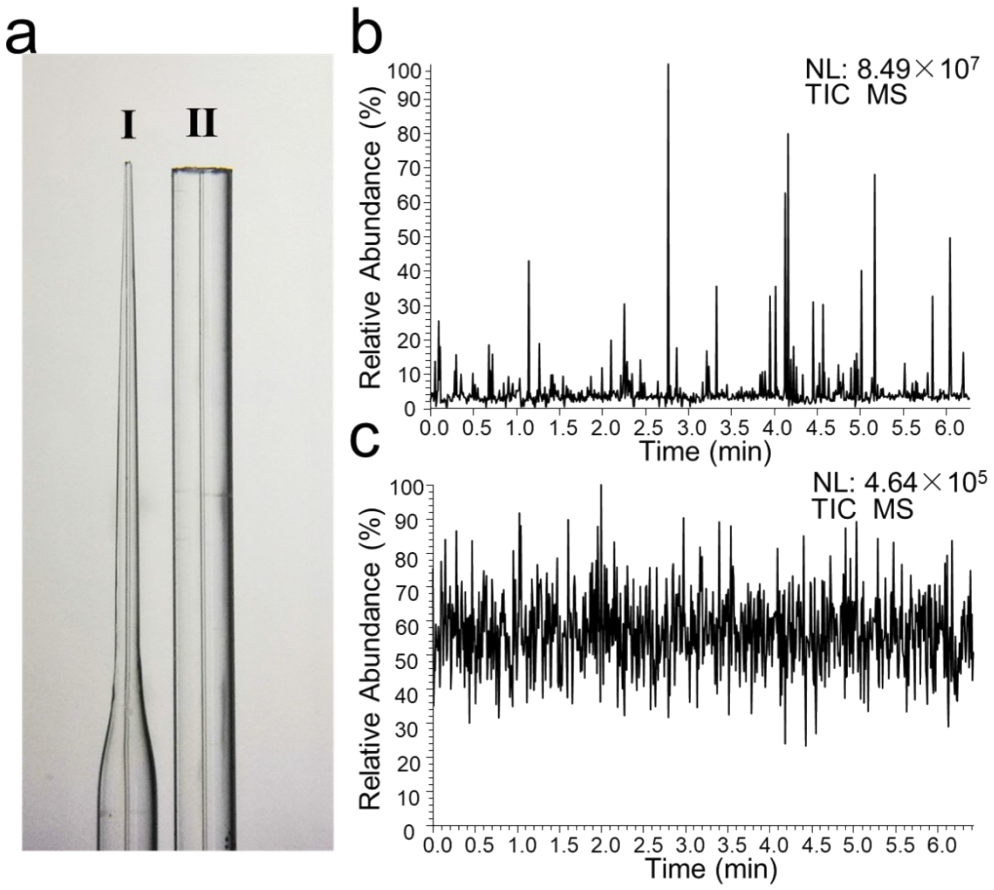

Figure S2. Effect of the presence or absence of a tip on the detection of KB cells by mass spectrometry. (a) The photo of two kinds of emitters; **(b)** Total ion chromatogram (TIC) of MS by capillary emitter I with a tip (the end outer diameter (O.D.) of 20 μm); **(c)** TIC of MS by capillary emitter II without a tip (the end O.D. of 340 μm).

The results show that a single-cell MS signal cannot be generated by a capillary without a tip, whereas an intense signal can be generated using a capillary with a tip. This result confirms that a capillary wall thinned by etching is necessary to generate a single-cell MS detection signal.

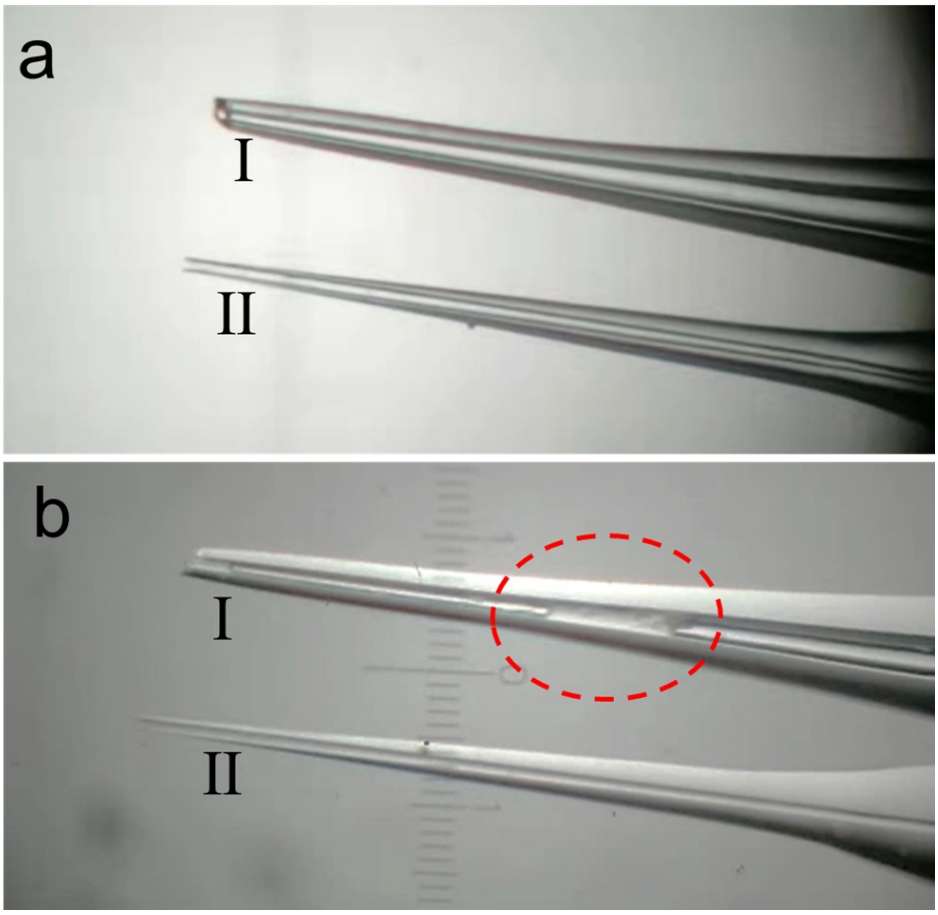

Figure S3. Comparison of the durability of the pulled and the etched tips. (a) Microscopic image of the emitters before infusion of cell suspension; **(b)** Microscopic image of the emitters after continuous infusion of cell suspension for 3 minutes.

The pulled tip (I) was prepared by a puller and broken under a microscope to obtain an open I.D. of ~16 μm. The constant-I.D. tip (II) was fabricated by the method developed by our group[1,2]; the I.D. of the tip was 16 μm. A549 cell suspension (the cell density is 5×10^5/mL) was used for the experiment, and the flow rate was 1 μL/min. After running for 3 minutes, emitter I became plugged (see the red circle), whereas emitter II remained unobstructed. This experimental result confirmed that the tip with a constant-I.D. has a low risk of fluidic clogging, enabling a stable flow rate and long operating life, which are important for high-throughput detection of complex biological samples.

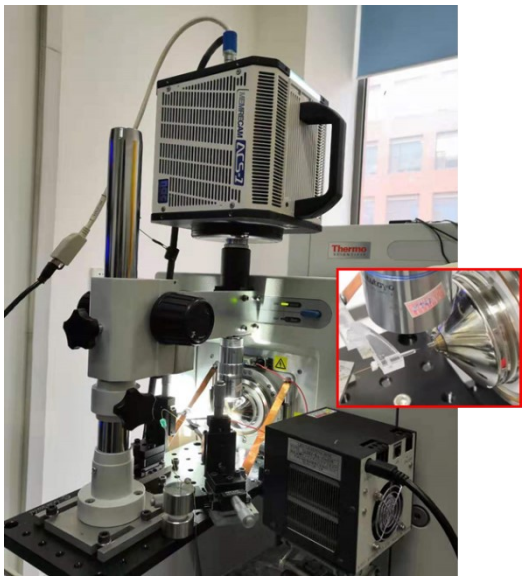

Figure S4. The photo of the ILCEI-MS on-line visualization platform. The platform comprised a self-designed and self-built ILCEI-MS ion source and a microscopic high-speed camera system composed of a long-distance microscope objective lens (50×, 0.42 NA, Mitutoyo, Japan) and a high-performance, high-speed camera (MEMRECAM ACS-3, NAC, Japan). The electrolaunching process of the tip during single-cell detection was visually recorded using this platform.

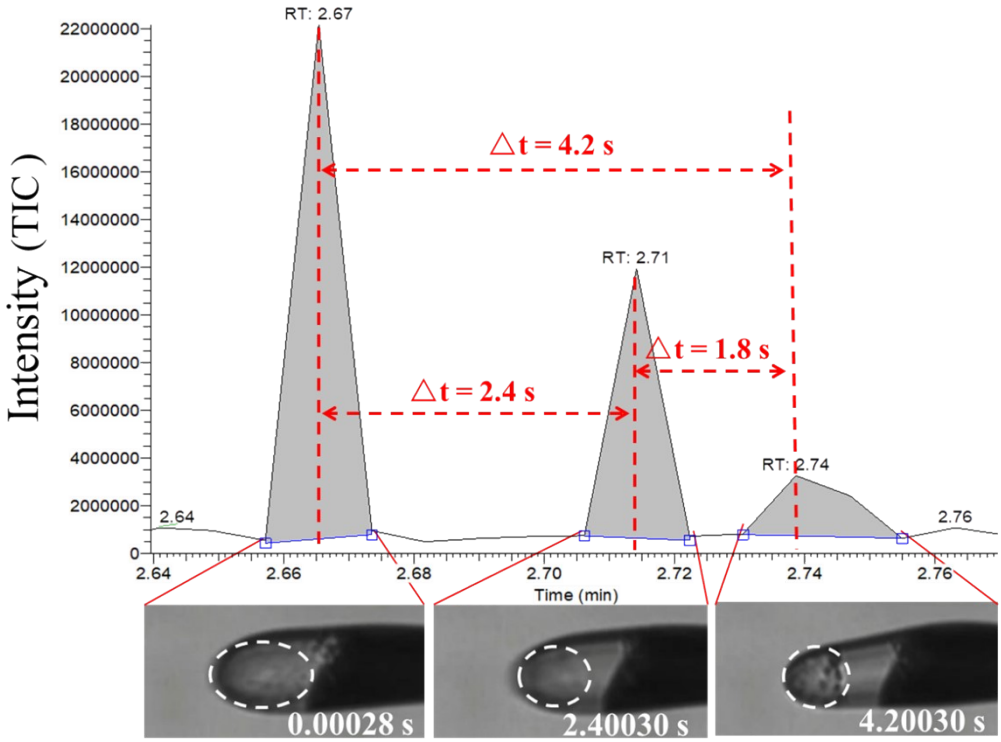

Figure S5. Single-cell participated in the electrolaunching process and the data collected synchronously by mass spectrometry.

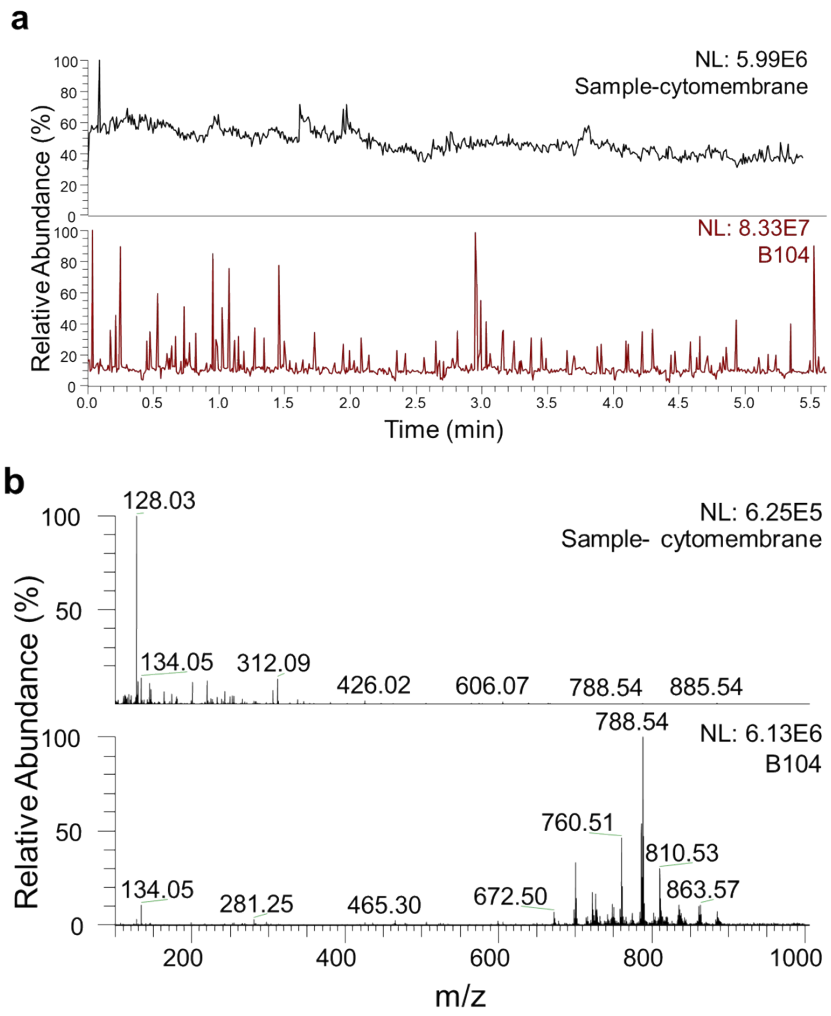

Figure S6. Mass spectrometry of cell membrane debris sample and intact living cell sample. **(a)** Comparison of TIC between the cell membrane debris sample (black line) and the intact living cell sample (red line); **(b)** Comparison of the mass spectra between the cell membrane debris sample (top) and the intact living cell sample (bottom). We used a Minute™ plasma membrane protein isolation kit to extract cell membranes in the bulk solution and mixed them with 40 mmol/L ammonium formate aqueous solution to prepare a sample of cell membrane debris. Mass spectrometry detection was performed under the same conditions for the cell suspension, and the difference of the mass spectrometric signals of the two samples was compared. It can be seen from **a** that there is no obvious spike in the TIC of the cell membrane debris sample, demonstrating that the ionization of cell membrane debris cannot cause the violent fluctuations of mass spectrometry signals like intact cells. As shown in **b**, the peak shape and ion intensity of the mass spectrum of the cell membrane debris sample are very different from the mass spectrometry signal of intact living single-cells. The ion intensity of the cell membrane debris sample is one order of magnitude lower than that of intact living single-cells. Even if large cell debris occasionally causes a signal peak similar to the signal peak appearing at 0.09 min in the TIC of the cell membrane debris sample. We set a threshold for single-cell data extraction, that is, only extracting peaks with a signal-to-noise ratio of more than 3.0 in the MS TIC. The extraction will further remove the influence of cell debris on the analysis results, ensuring that our subsequent analysis data come from intact single-cells.

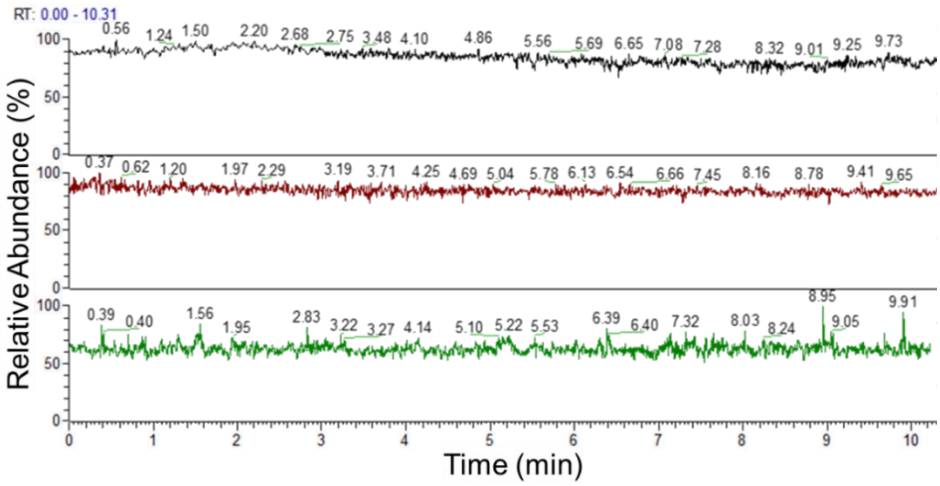

Figure S7. MS's TIC of the perfusion injection of three kinds of samples. From top to bottom are 40 mmol/L ammonium formate aqueous solution (black line), the cell lysate of lung cancer cells (red line, the collected supernatant after the centrifugation at 17,000 g), the liposome suspension with an average diameter of 200 nm (green line). There is no obvious spike in TICs of the three kinds of samples.

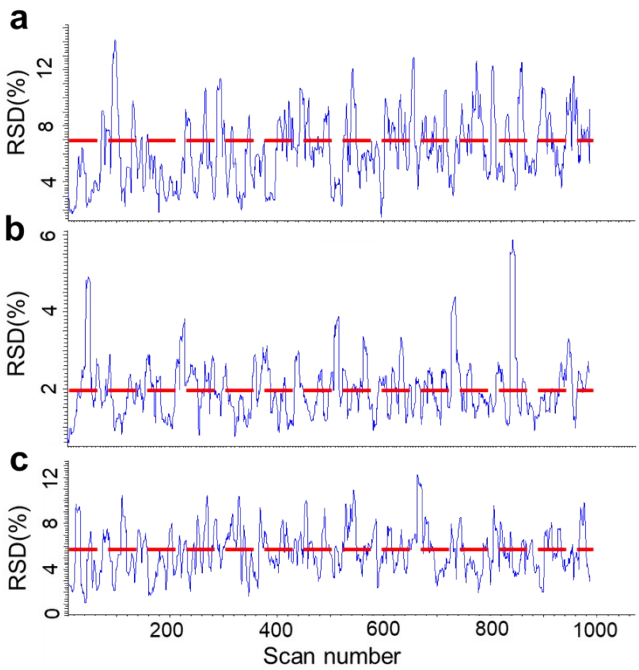

Figure S8. The relative standard deviation (RSD) of 1000 scans of the mass spectrum signal. **(a)** 40 mmol/L ammonium formate aqueous solution; **(b)** Signal of the cell lysate of lung cancer cells; **(c)** Signal of the liposome suspension with an average diameter of 200 nm. The red dotted line represents the average RSD. The RSD data come from the built-in function of the LTQ-Orbitrap XL mass spectrometer, which is used to evaluate the stability of the ion source before the instrument is calibrated. Technical specifications require that the average RSD value of 100 scans is less than 15% for mass spectrometer calibration. We collected 1000 scans, and the average RSD value is less than 7%, reaching the signal stability level that can be used for mass spectrometer calibration, which proves that the system stability of this method is reliable.

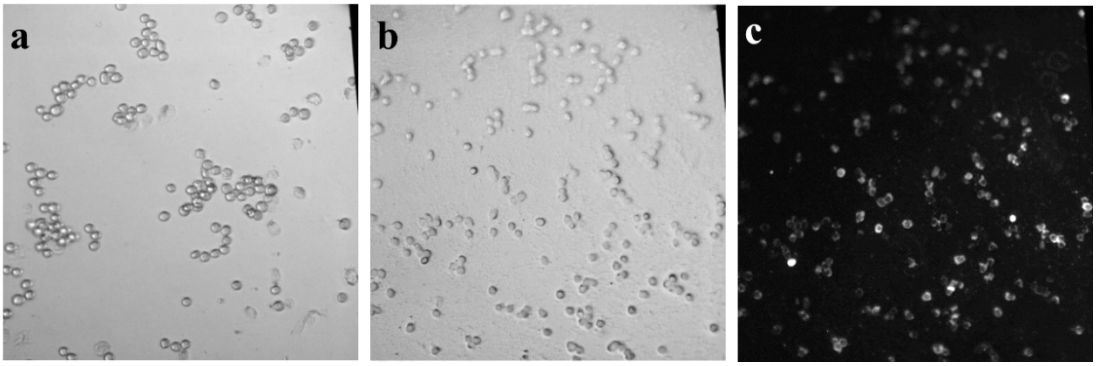

Figure S9. Comparison of cells status before and after electrolaunching. (a) Cells suspended in 40 mmol/L ammonium formate aqueous solution before electrolaunching; **(b)** Cells collected at the inlet of the mass spectrometer (bright-field imaging); **(c)** Cells collected at the inlet of the mass spectrometer (fluorescence imaging, by DiO cell membrane green fluorescent probe stained). It can be seen that all the fluorescence signals come from the intact cells, and no luminous cell debris is seen. It means that most of the cells still maintained a complete structure.

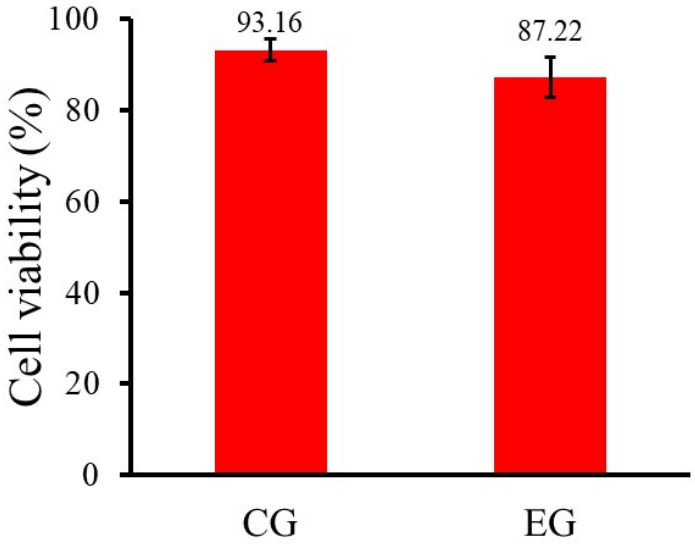

Figure S10. Cell viability verification by CCK8. CG (control group): The cells that underwent the sample preparation process from ILCEI-MS. EG (experimental group): The cells collected near the mass spectrometry ion entrance. Cells without any treatment were used as the blank group, of which cell viability is considered to be 100%. The data show that most cells still maintained an alive status.

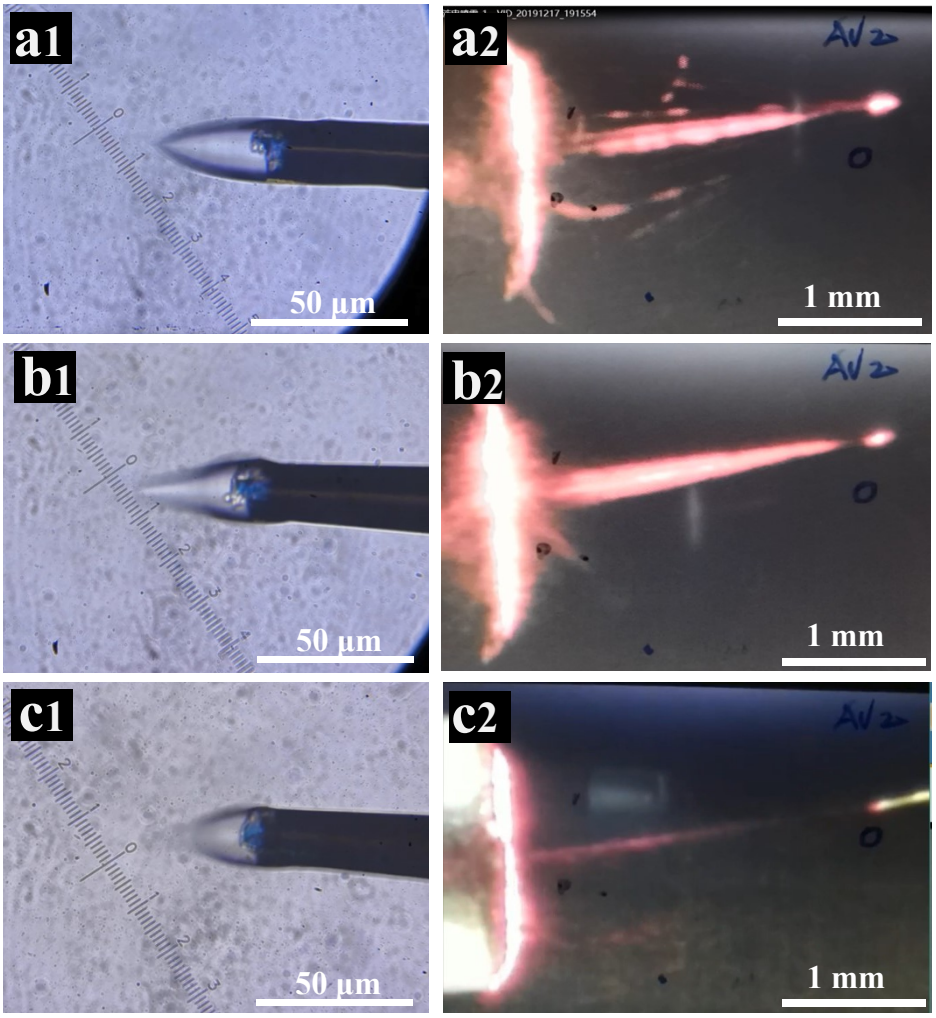

Figure S11. Comparison of the mass spectrometry injection status of different solutions under the same conditions. (a1, b1, and c1) High-speed camera screenshots of the liquid cones. **(a2, b2, and c2)** High-speed screenshots of the plume morphology. **(a1**, **a2)** The electrospray status with a methanol aqueous solution (70% v/v); **(b1, b2)** The electrospray status with an aqueous solution; **(c1, c2)** The electrolaunching status with a suspension of A549 cells suspension. A constant-I.D. emitter of 16/20 μm (I.D./O.D.) with a thin-wall tip was used; the injection current was approximately 0.3 μA to ensure that the initial droplets carried an equal amount of charge per unit time, and the distance between the emitter and ion inlet was 3 mm.

To further investigate the ionization characteristic of ILCEI, we observed the plume morphology. The three liquids produced hydraulic cones of different shapes at the same launching / spray current (approximately 30 μA to ensure that the initial droplets carried an equal amount of charge per unit time); this phenomenon intuitively proves that the plume morphology of the three liquids is different. But the more important difference was that the initial droplets of the three liquids produced diverse fragmentation in the air flight zone (**a2**, **b2** and **c2**). According to the Rayleigh limit theory [5], the net charge Q_R of a charged droplet should satisfy the equation:

$$Q_R = 8\pi(\varepsilon_0 \gamma r_0^3)^{1/2}$$

where ε_0 is the vacuum permittivity, γ is the surface tension, and r_0 is the radius of the droplet. With the same net charge, droplets formed with a high proportion of methanol solution had a low surface

tension and were more likely to reach the Rayleigh limit and split. Therefore, **a2** spray plume was larger than **b2**. The results shown in **b2** and **c2** were obtained under the same liquid mobile phase conditions and should, in theory, have roughly the same liquid surface tension. However, the A549 cell suspension exhibited less droplet splitting (**c2**) because of the presence of whole cells in the initial droplets of the cell suspension for electrolaunching, which hindered droplet shrinkage. The maintained large surface area avoided reaching the Rayleigh limit and thus prevented the droplets from splitting. Because droplet splitting was accompanied by a random distribution of net charge, decreased droplet splitting would result in more charge remaining on the surface of the mother droplet. In addition, very few mobile phases mean very few impurity molecules in the mother liquid droplets. Thus, cell components retained in the mother droplet will have a greater chance of gaining charge and thus achieve more adequate ionization. All cell components enter the entrance of the mass spectrometer, thus avoiding the loss of the sample in the atmospheric path and improving the sample collection rate. For a homogeneous solution, the sample molecules are always accompanied by a large number of solvent molecules during the multiple splitting process of charged droplets, so there is fierce competition for charges between a large number of impurities and a small number of samples. Coupled with the dilution and annihilation of sample ions in the atmosphere, and the very low ion acquisition ratio at the MS inlet, these have led to a serious decrease in the detection sensitivity of the sample.

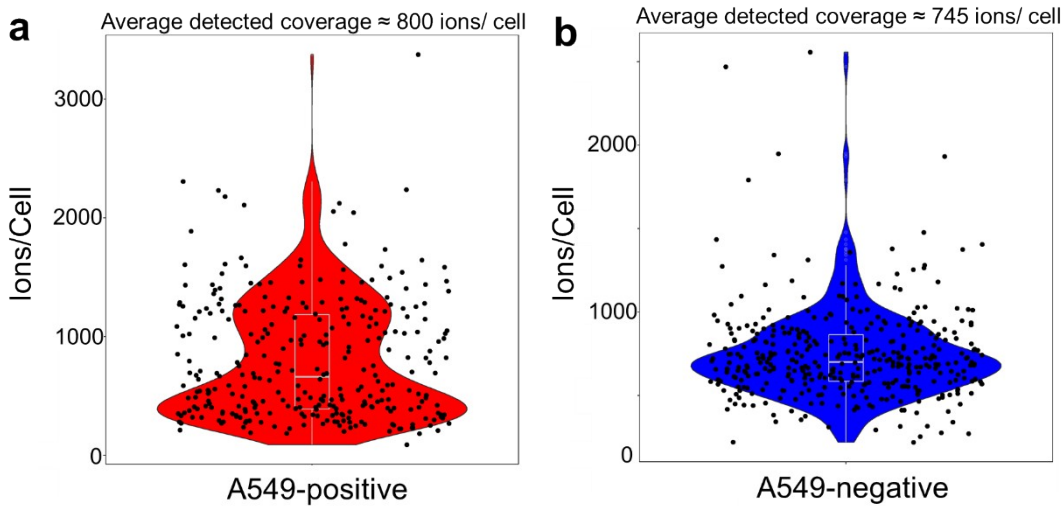

Figure S12. Violin plots of ions per cell in ILCEI-MS dataset of living A549 cells. Each dot represents a single-cell. **(a)** 306 living A549 cells were detected in positive ion mode, and the average detected coverage is about 800 ions/cell; **(b)** 376 living A549 cells were detected in negative ion mode, and the average detected coverage is about 745 ions/cell.

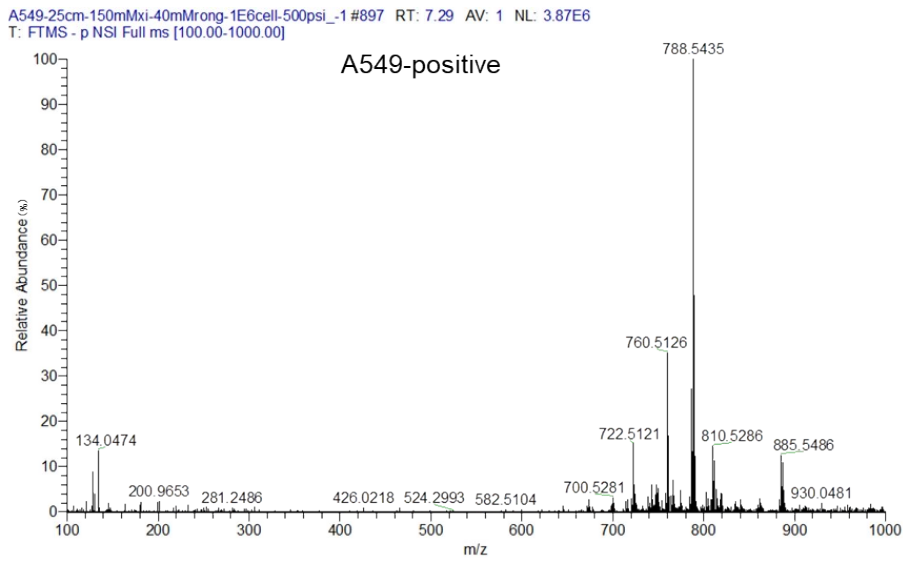
A549-25cm-150mMxi-40mMrong-1E6cell-500psi_-1 #897 RT: 7.29 AV: 1 NL: 3.87E6
T: FTMS - p NSI Full ms [100.00-1000.00]
A549-positive
Relative Abundance (%)
m/z
788.5435
760.5126
722.5121
810.5286
885.5486
930.0481
700.5281
134.0474
200.9653
281.2486
426.0218
524.2993
582.5104

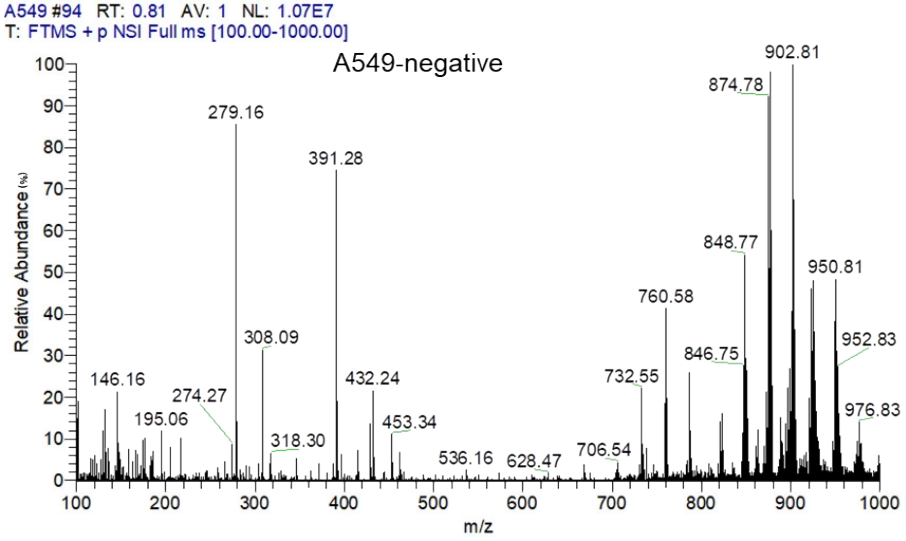
A549 #94 RT: 0.81 AV: 1 NL: 1.07E7
T: FTMS + p NSI Full ms [100.00-1000.00]
A549-negative
Relative Abundance (%)
m/z
902.81
874.78
279.16
391.28
848.77
950.81
760.58
952.83
308.09
846.75
146.16
274.27
432.24
732.55
976.83
195.06
453.34
318.30
536.16
628.47
706.54

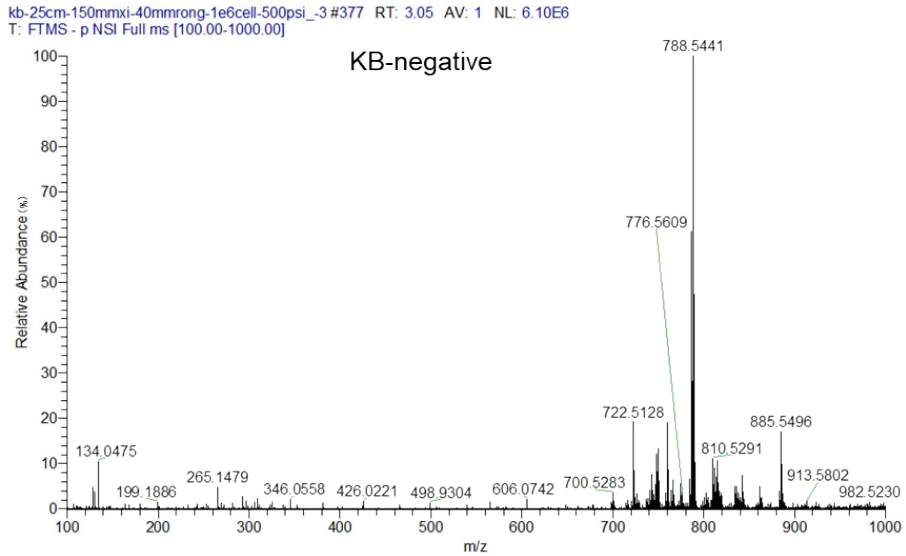
kb-25cm-150mmxi-40mmrong-1e6cell-500psi_-3 #377 RT: 3.05 AV: 1 NL: 6.10E6
T: FTMS - p NSI Full ms [100.00-1000.00]
KB-negative
Relative Abundance (%)
m/z
788.5441
776.5609
722.5128
885.5496
810.5291
134.0475
913.5802
265.1479
199.1886
346.0558
426.0221
498.9304
606.0742
700.5283
982.5230

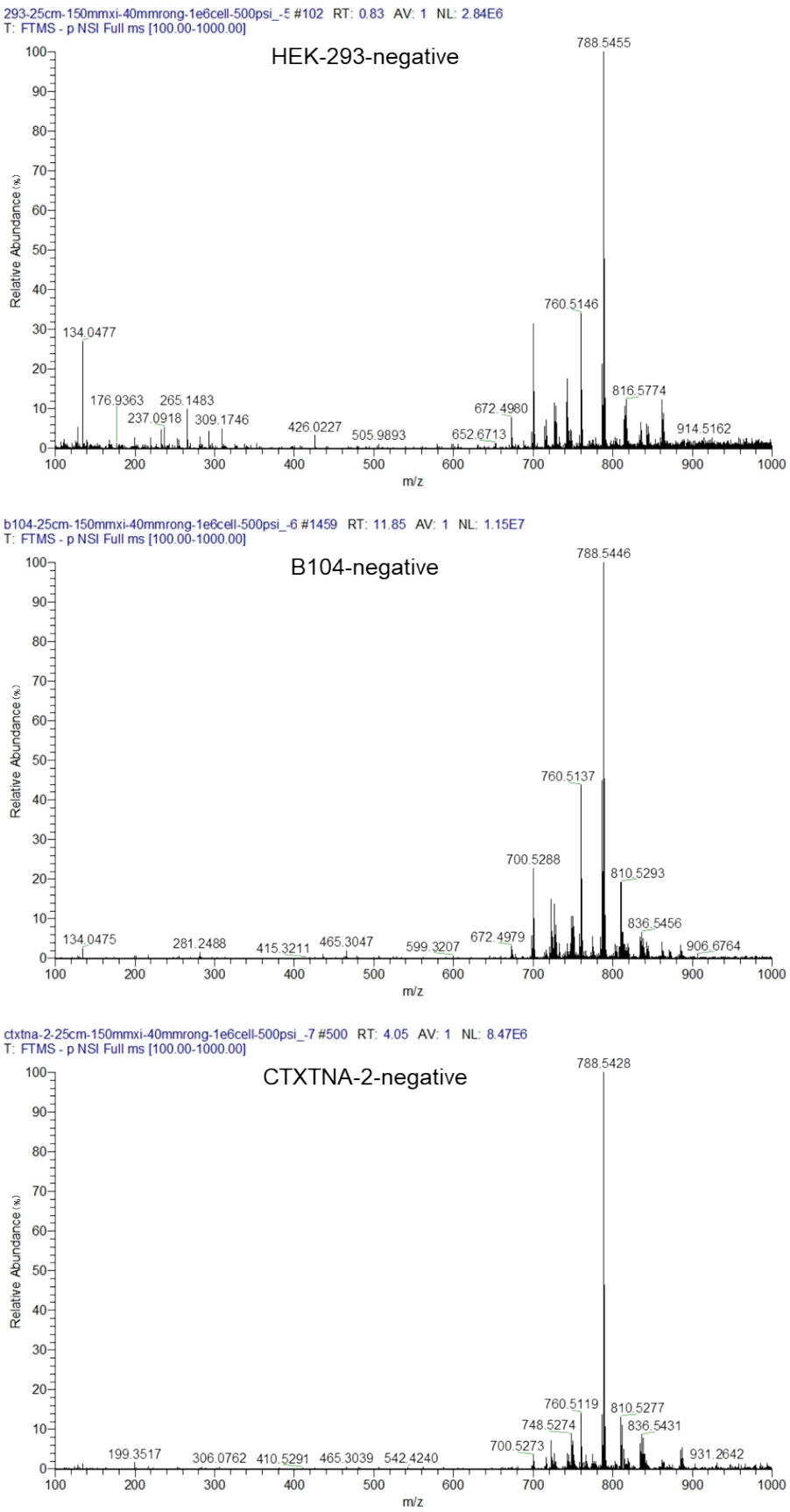

Figure S13. Single-cell mass spectra of five different types of cells (A549, KB, HEK-293, B104, and CTXTNA-2).

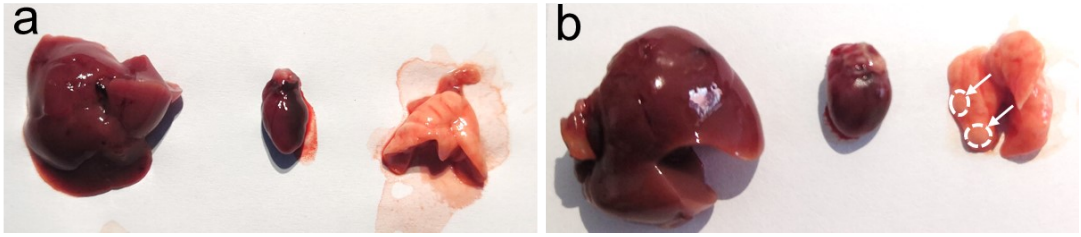

Figure S14. Photographs of the liver, heart, and lung (from left to right) of the dissected mice. **(a)** Healthy mouse; **(b)** Lung cancer mouse. The lung masses (the white dotted circle indicated by the arrow) of the lung cancer mouse were obvious, and the liver was enlarged and hard, indicating that the mouse had shown obvious symptoms**.**

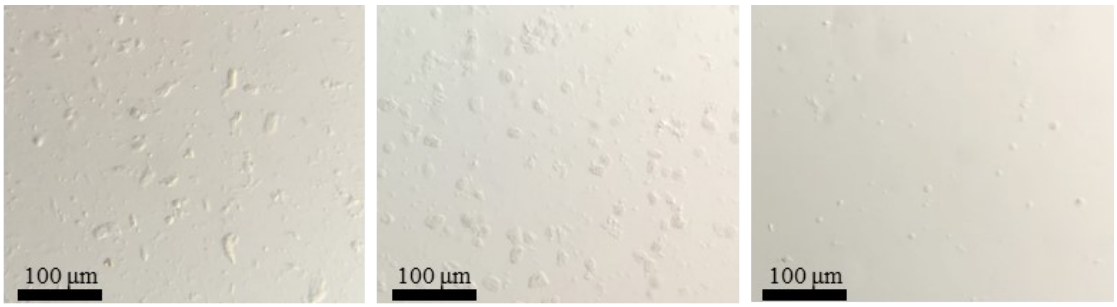

Figure S15. The cell suspensions of visceral digestion from a healthy mouse. Suspensions of heart, liver, and lung cells are shown from left to right successively.

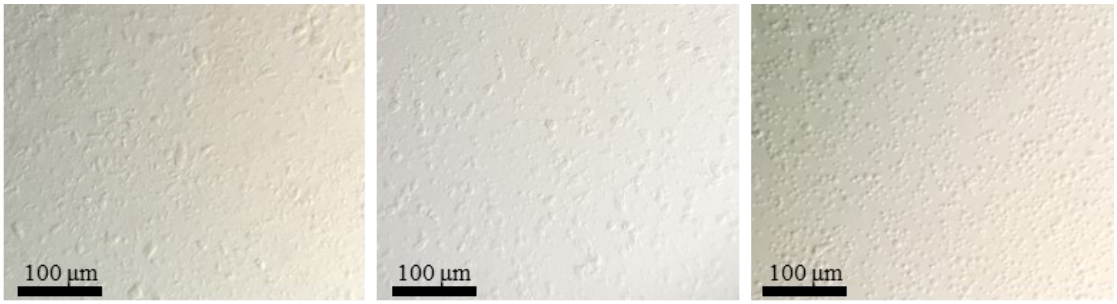

Figure S16. The cell suspensions of visceral digestion from a lung cancer mouse. Suspensions of heart, liver, and lung cells are shown from left to right successively.

It was found that the single-cells obtained from the heart and liver were larger in volume through microscopic observation; therefore, in this part of the experiment, a 25 μm I.D. capillary was used to complete the separation, transport, and electron-emission ionization mass spectrometry detection of the single-cells.

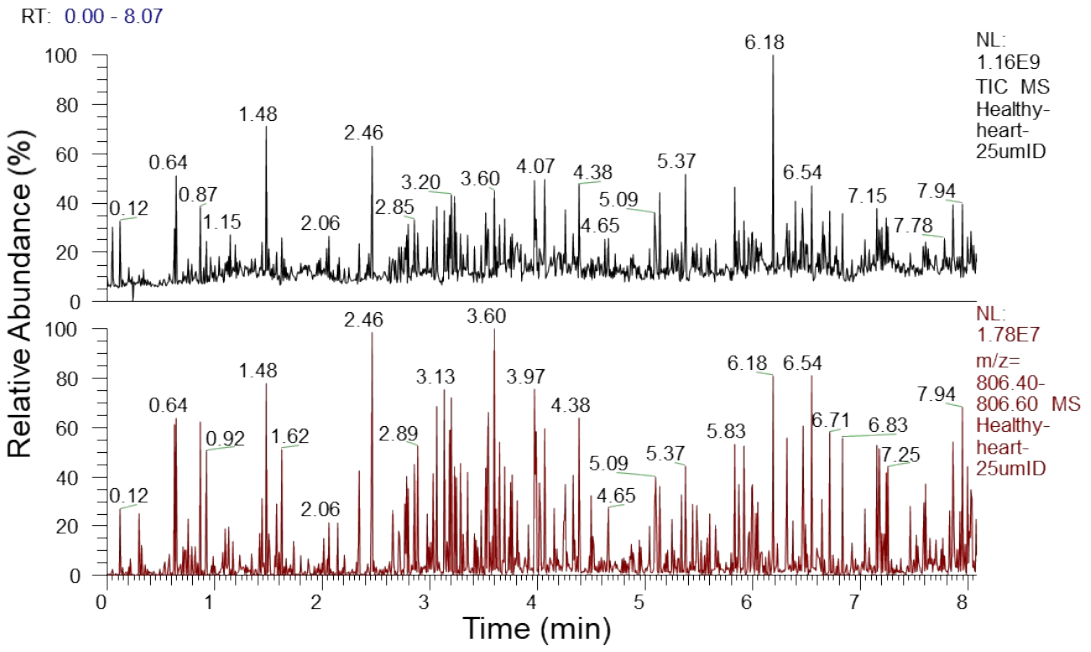

Figure S17. ILCEI-MS data of cell suspension digested from the heart of a healthy mouse. From top to bottom are TIC and EIC, respectively. EIC extracted based on *m/z* 806.40–806.60, which acts as the reference of single-cell data.

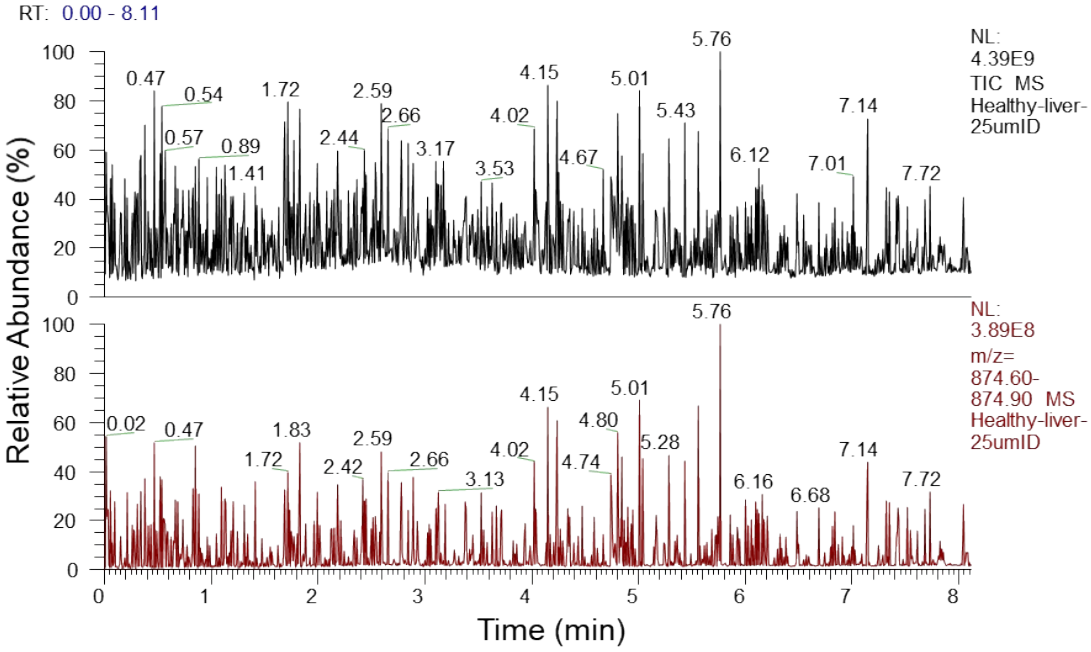

Figure S18. ILCEI-MS data of cell suspension digested from the liver of a healthy mouse. From top to bottom are TIC and EIC, respectively. EIC extracted based on *m/z* 874.60–874.90, which acts as the reference of single-cell data.

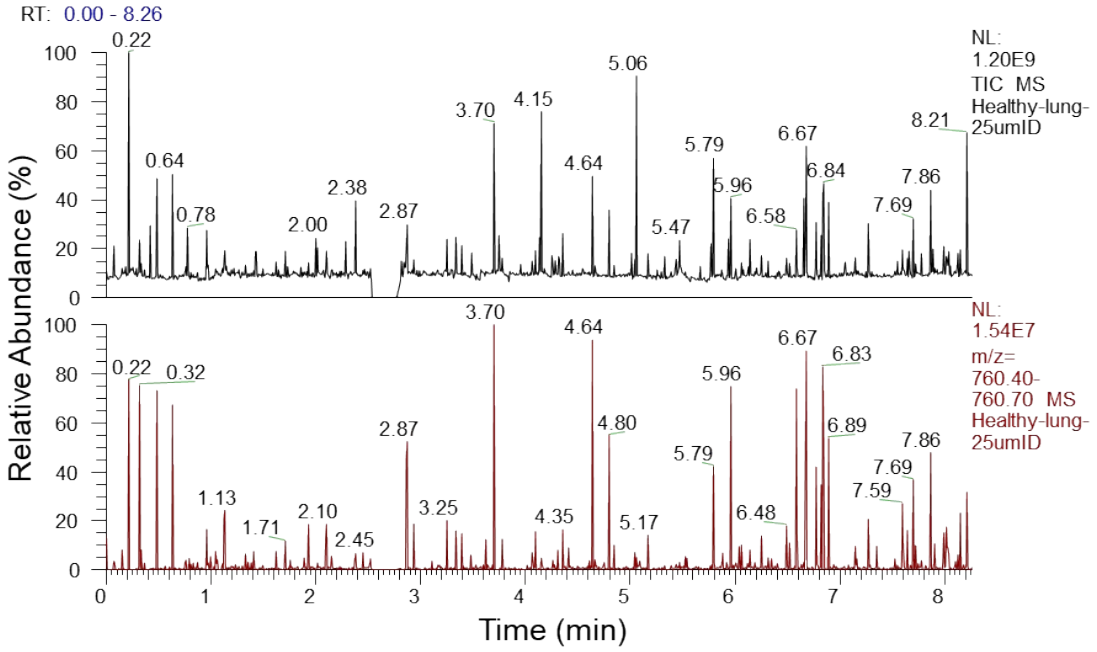

Figure S19. ILCEI-MS data of cell suspension digested from the lung of a healthy mouse. From top to bottom are TIC and EIC, respectively. EIC extracted based on *m/z* 760.40–760.70, which acts as the reference of single-cell data.

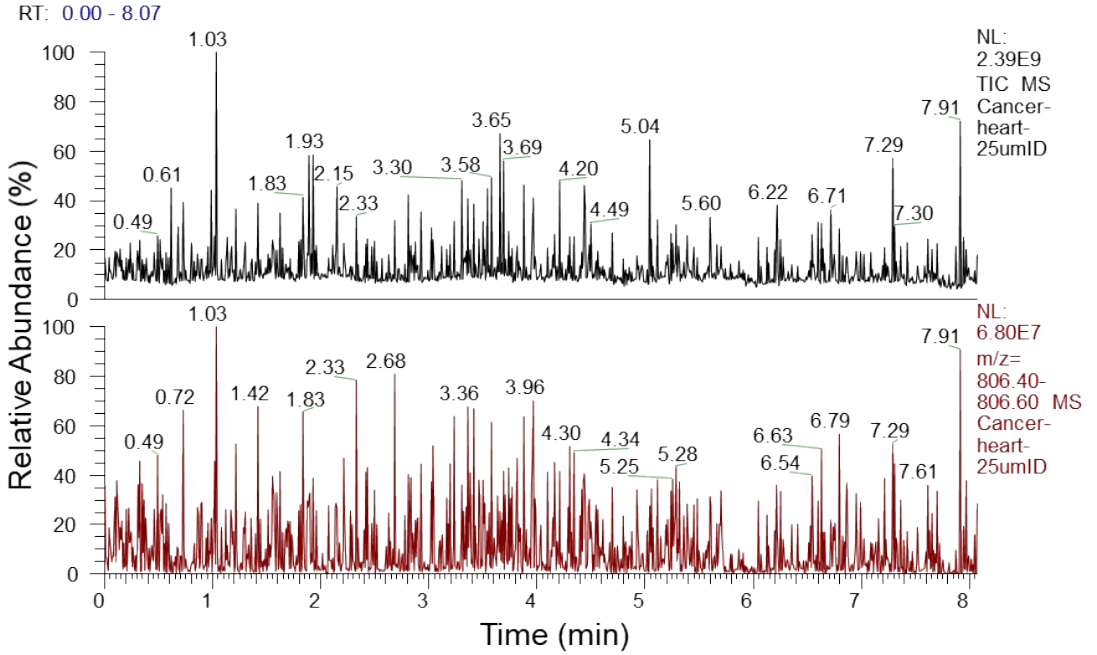

Figure S20. ILCEI-MS data of cell suspension digested from the heart of a lung cancer mouse. From top to bottom are TIC and EIC, respectively. EIC extracted based on *m/z* 806.40–806.60, which acts as the reference of single-cell data.

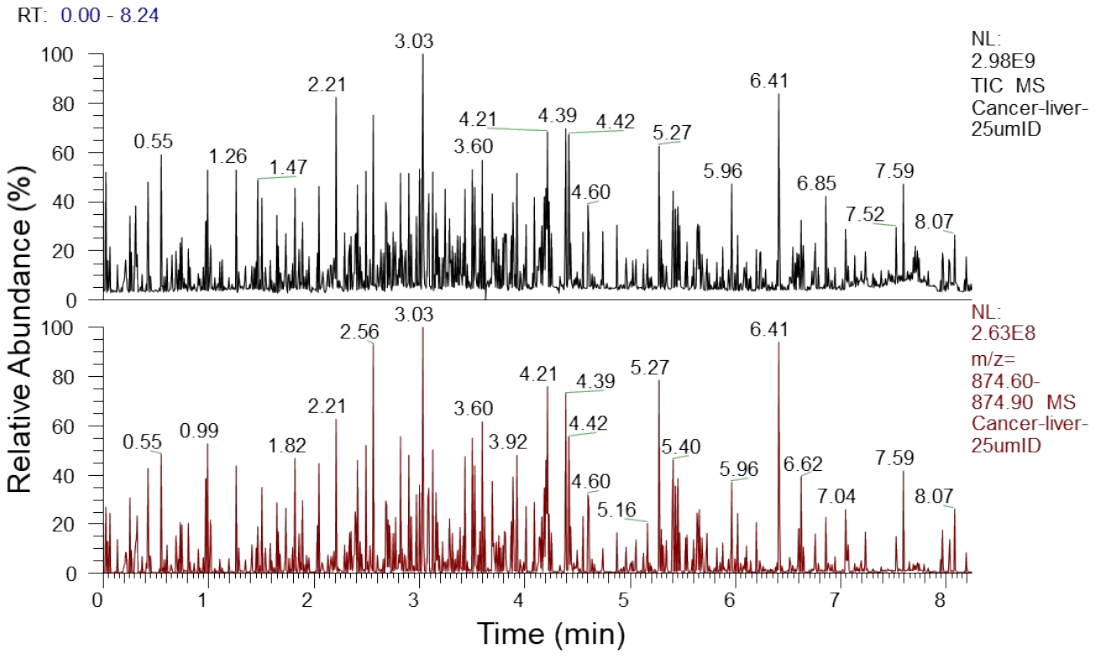

Figure S21. ILCEI-MS data of cell suspension digested from the liver of a lung cancer mouse. From top to bottom are TIC and EIC, respectively. EIC extracted based on *m/z* 874.60–874.90, which acts as the reference of single-cell data.

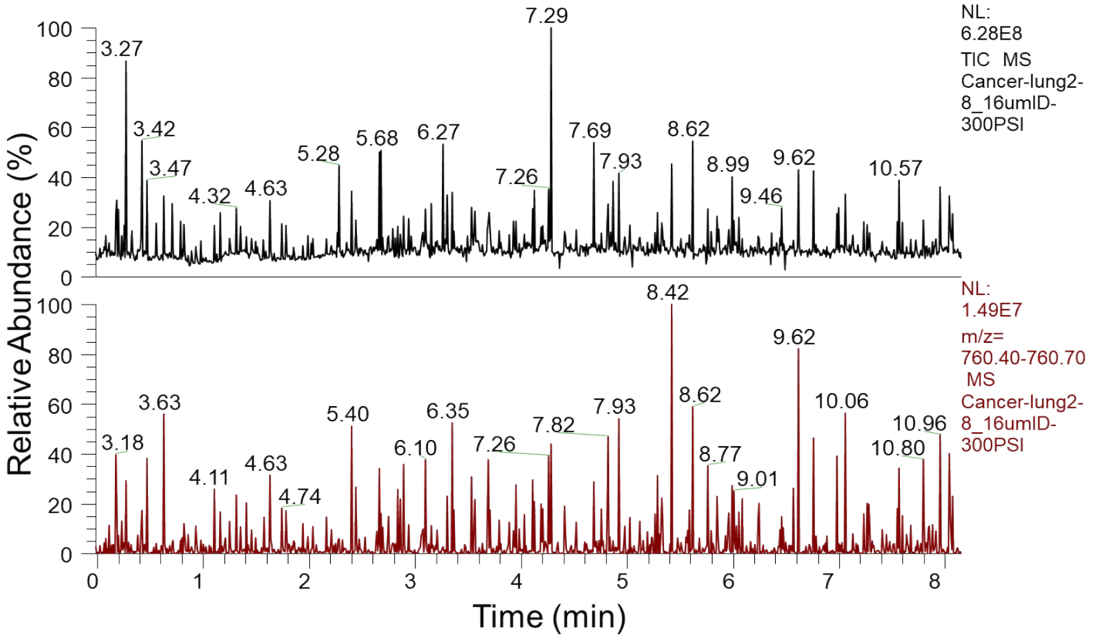

Figure S22. ILCEI-MS data of cell suspension digested from the lung of a lung cancer mouse. From top to bottom are TIC and EIC, respectively. EIC extracted based on *m/z* 760.40–760.70, which acts as the reference of single-cell data.

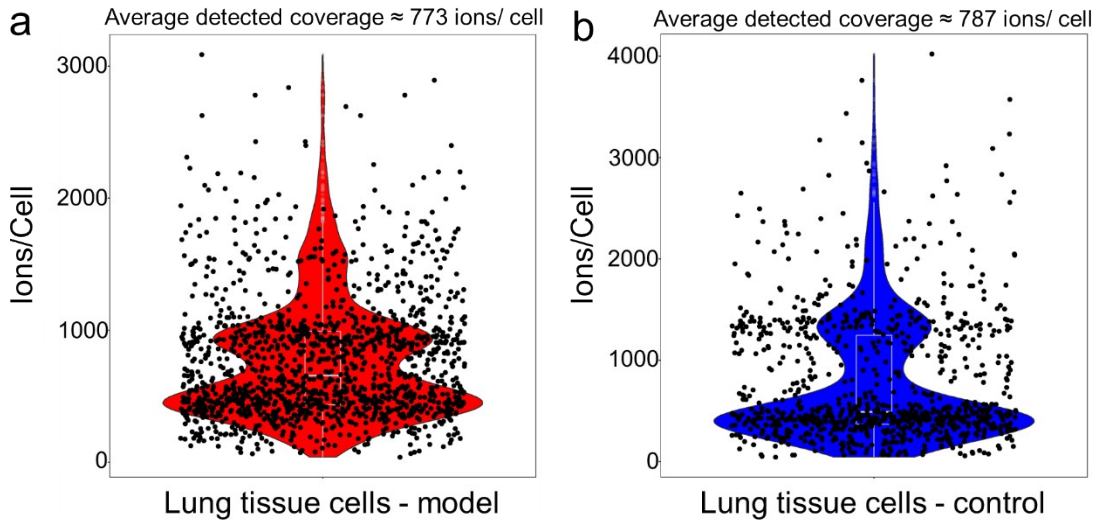

Figure S23. Violin plots of ions per cell in ILCEI-MS dataset of lung tissue cells of lung cancer model mice and healthy mice. Each dot represents a single-cell. **(a)** 1438 cells were detected from the lung tissue of lung cancer model mice, and the average detected coverage is about 773 ions/cell; **(b)** 930 cells were detected from the lung tissue of healthy mice, and the average detected coverage is about 787 ions/cell.

3. Supplementary Videos

Video S1. At a shooting speed of 10000 frames/s and a magnification of 500x, the motion of an A549 cell in a 16 μm I.D. capillary.

Individual A549 cells can be seen in the narrow capillary being squeezed into an oval shape and moving towards the capillary outlet. This vivid scene strongly proves the excellent single-cell separation and transportation capacity of the narrow-bore capillary.

Video S2. At a shooting speed of 10000 frames/s and a magnification of 200x, the motion of multiple A549 single-cells moves independently and orderly in a 16 μm I.D. capillary.

It further fully demonstrates the excellent single-cell separation and transportation capability of the narrow-bore capillary. The scale bar in the video is 100 μm.

Video S3. At a shooting speed of 50000 frames/s and a magnification of 500x, the whole A549 single-cell droplets producing process by narrow capillary emitter with constant-I.D. throughout the column.

In negative ion mode, the electrolaunching voltage is 1.36 kV, the I.D./O.D. of the emitter is 16/20 μm, the liquid phase is 40 mmol/L ammonium formate aqueous solution, and the flow rate is 1 μL/min. The video material clearly shows the formation of single-cell droplets. We can clearly see that most of the volume of the droplets is occupied by an integrate single A549 cell, and only an ultra-thin layer liquid film on the periphery is composed of the liquid phase. This fully proves the conclusion that the single-cell droplet hardly introduces the sample dilution.

Video S4. Video recording of the working scene of ILCEI-MS characterized by high-speed camera online visualization.

It can be seen that the high-speed camera and mass spectrometry data acquisition are synchronized according to the video.

Video S5. The integrated video of high-speed camera acquired in supplementary video S4 and synchronous acquired mass spectrometry data.

It can be found that the interval generated by three successive single-cell droplets and the interval of retention time of three independent signal peaks collected by the mass spectrum are perfectly matched. Those prove that each signal peak in the total ion chromatograms obtained by ILCEI-MS is from one single-cell.

Video S6. At a shooting speed of 50000 frames/s and a magnification of 200x, the integrated video of three videos of single-cell droplets generating, flying in the atmosphere, and entering into the MS inlet.

From the video, we can clearly see that pulsed droplets with uniform diameter are produced by the novel single-cell droplet electrolaunching mode and these droplets do not split obviously during the flight in the atmosphere and enter into the MS inlet in the form of an intact structure, which vividly demonstrates features of the new electrolaunching technology proposed in this work. It also strongly proves our conclusion that an in-source ionization occurs by single-cell droplets. The scale

bar in the video is 100 μm.

Video S7. Comparison of electrolaunching / spray images of cell suspensions by using constant-I.D. narrow capillary emitters with different outer diameters under the same voltage parameter.

By comparison of emitters with 16 μm I.D. and different outer diameters, we find that the emitter with 20 μm O.D. can produce single-cell droplets with almost zero dilution, while the cells are stuck in the emitter cone of the 80 μm O.D. emitter stays and are difficult to eject. This data illustrates that the single-cell electrolaunching mode proposed in this work needs to be based on thin-wall emitters. The scale bar in the video is 100 μm.

Video S8. The difference between the ionization states of ILCEI and ESI.

The video file includes three columns. From left to right are event A of 40 mmol/L ammonium formate in methanol (v/v: 70/30) solution, event B of 40 mmol/L ammonium formate solution, and event C of A549 cells suspended in 40 mmol/L ammonium formate aqueous solution. Each event contains two kinds of characterization results of the same scene captured by a high-speed microscope camera (top) and a commercial Nano-ESI camera under laser irradiation (bottom). From the video, it can be seen that cell suspension C has the shortest electrolaunching cone length; the formed droplets fly through the atmosphere into the ion transfer tube along a very thin straight line. The difference between B and C illustrates the difference between single-cell droplets and ordinary charged droplets in the ionization process. That is, single-cell droplets do not undergo a droplet splitting in the atmosphere (charged droplet splitting is a prerequisite for ionization in ESI theory). This set of data intuitively shows that the ILCEI is indeed a new mode different from the ESI, and also supports the inference that single-cell droplets are ionized within the inlet of the mass spectrometer.

4. Supplementary Table.

Table S1. The velocity of the single-cell and average shear stress of wall surface on the single-cell at the outlet of capillary emitters with different I.D..

Emitter I.D. (μm)	**Exit velocity (m/s)**	**Average shear stress (Pa)**
16	0.083	0.04
50	0.0085	0.0006
100	0.00212	0.00016

Table S2. 368 cellular metabolites were identified for A549 cells, 249 and 119 in positive and negative ion modes, respectively (scan range *m/z* 100–1000). For the detection of metabolite extract from population cells, $ddMS^2$ mode with higher energy collisional dissociation (HCD) was used. The metabolites extracted from population cells were initially identified by searching mzCloud Advanced Mass Spectral Database (https://www.mzcloud.org/) with MS/MS fragments. Selected top five candidates were further verified through matching the Human Metabolome Database 5.0 (HMDB) (http://www.hmdb.ca/) and MassBank Database 2.1.8 (http://www.massbank.jp/Index). The metabolites with the same molecular weight could not be separated by existing methods. Therefore, the metabolite would remain if characteristic product ions were contained in the MS/MS fragments. If the intensities of all characteristic product ions of the metabolite were less than 10%, the metabolite would be ignored. Non-endogenous components are not excluded from the list.

NO.	Metabolites	Formula	m/z	Mass	Ions	CAS_ID	HMDB_ID	KEGG_ID	MS/MS fragments
Positive ion mode									
1	2-Piperidinone	C_5H_9NO	100.0750	99.1311	M+H	675-20-7	HMDB0011749	—	81.68;71.80
2	2,3-Dihydrobenzofuran	C_8H_8O	103.0500	120.0575	M+H-H_2O	496-16-2	HMDB0013815	—	77.0382;53.0382;51.801
3	Pentanoic acid	$C_5H_{10}O_2$	103.0750	102.0681	M+H	109-52-4	HMDB0000892	C00803	50.666;70.9794;54.6772
4	N-Methylalanine	$C_4H_9NO_2$	104.0700	103.0633	M+H	3913-67-5	HMDB0094692	—	72.3887
5	Gamma-Butyrolactone	$C_4H_6O_2$	104.0700	86.0368	M+NH_4	96-48-0	HMDB0000549	C01770	66.0566;86.096
6	4-Aminobutanoic acid	$C_4H_9NO_2$	104.0700	103.0633	M+H	—	HMDB0000112	C00334	84.0792;86.0961
7	Choline	$C_5H_{14}NO$	104.1071	104.1075	M+	62-49-7	HMDB00097	C00114	60.1
8	2-Phenylethanol	$C_8H_{10}O$	105.0540	122.0732	M+H-H_2O	1960/12/8	HMDB0033944	C05853	79.0538;77.0382;66.0567
9	Ethylbenzene	C_8H_{10}	107.0856	106.0777	M+H	100-41-4	HMDB59905	C07111	75.0229;91.0542
10	O-Toluidine	C_7H_9N	108.0441	107.1531	M+H	95-53-4	HMDB0041965	C14403	107.83;92.76;91.03
11	2,5-Dimethylpyrazine	$C_6H_8N_2$	109.0764	108.1411	M+H	123-32-0	HMDB0035289	—	80.89;66.81
12	Glycerol	$C_3H_8O_3$	110.0816	92.0473	M+NH_4	56-81-5	HMDB00131	C00116	75.0441

13	5-Methyl-2-furancarboxaldehyde	$C_6H_6O_2$	111.0441	110.0363	M+H	620-02-0	HMDB33002	—	83.0491;93.0335
14	1-(Aminomethyl)phosphonic acid	CH_6NO_3P	112.0010	111.0085	M+H	1066-51-9	HMDB0247130	C11033	78.4077
15	Dimethyl sulfone	$C_2H_6O_2S$	112.0420	94.0089	$M+NH_4$	67-71-0	HMDB0004983	C11142	84.0805;78.4075;70.0649
16	Cytosine	$C_4H_5N_3O$	112.0506	111.0427	M+H	71-30-7	HMDB00630	C00380	69.0453;95.0245
17	Methyl-L-proline	$C_6H_{11}NO_2$	112.0750	129.0790	$M+H-H_2O$	68078-09-1	HMDB0094696	—	84.0805;70.0649
18	Pipecolic acid	$C_6H_{11}NO_2$	130.0483	129.1570	M+H	3105-95-1	HMDB0000070	C00408	129.96;83.77;73.86
19	Epsilon-caprolactam	$C_6H_{11}NO$	114.0901	113.1576	M+H	105-60-2	HMDB0062769	C06593	96.94;71.86
20	Methylsuccinic acid	$C_5H_8O_4$	115.0360	132.0423	$M+H-H_2O$	498-21-5	HMDB0001844	—	86.0598
21	Cis-Acetylacrylate	$C_5H_6O_3$	115.0392	114.0312	M+H	—	HMDB60461	C07091	69.0335
22	Proline	$C_5H_9NO_2$	116.0700	115.0633	M+H	147-85-3	HMDB0000162	C00148	70.0647
23	3-Phenylpropanal	$C_9H_{10}O$	117.0540	134.0732	$M+H-H_2O$	104-53-0	HMDB0033716	—	71.0681;91.0539;66.0568
24	Dihydrocarvone	$C_{10}H_{16}O$	117.1020	152.1201	$M+H-2H_2O$	5524-05-0	HMDB0036079	C11398	91.0539;66.0568
25	Betaine	$C_5H_{11}NO_2$	118.0860	117.0790	M+H	107-43-7	HMDB0000043	C00719	72.0804;92.0572
		$C_5H_{11}NO_2$	140.0680	117.0790	M+Na				
26	Pyrrolidine	C_4H_9N	118.0860	71.0735	M+HCOO+2H	123-75-1	HMDB0031641	—	72.0805
27	4-Propylphenol	$C_9H_{12}O$	119.0700	136.0888	$M+H-H_2O$	645-56-7	HMDB0032625	C14311	91.0539;104.0617
28	3-Hydroxy-3-methylbutanoic acid	$C_{25}H_{36}O_9$	119.0706	118.0625	M+H	96681-66-2	HMDB33654	—	91.0542
29	Pralidoxime	$C_7H_8N_2O$	120.0650	136.0637	$M+H-H_2O$	154-97-2	HMDB0014871	C07400	103.0539;91.0539;77.0383
30	Homoserine	$C_4H_9NO_3$	120.0658	119.0577	M+H	672-15-1	HMDB00719	C00263	102.091
		$C_4H_9NO_3$	256.1390	119.0577	$2M+NH_4$				102.091;88.0754;70.0648

31	2-Hydroxyphenethylamine	$C_8H_{11}NO$	120.0805	137.0841	M+H-H_2O	7568-93-6	HMDB0001065	C02735	103.0539;91.0539;77.0382
32	Tyramine	$C_8H_{11}NO$	120.0808	137.0841	M+H-H_2O	51-67-2	HMDB0000306	C00483	105.0444;91.0539;77.0382
33	2-Hydroxynicotinic acid	$C_6H_5NO_3$	122.0270	139.0269	M+H-H_2O	609-71-2	HMDB0059710	—	66.0566;92.0571
34	Ethylaniline	$C_8H_{11}N$	122.0960	121.0891	M+H	103-69-5	HMDB0302429	C14455	81.0444;66.0565;72.3884
35	Hydroxyurea	$CH_4N_2O_2$	123.0300	76.0273	M+HCOO+2H	127-07-1	HMDB0015140	C07044	77.0382
36	Nicotinamide (Vitamin B3)	$C_6H_6N_2O$	123.0440	122.0480	M+H	98-92-0	HMDB0001406	C00153	80.0491;95.0488;105.0444
37	4-Methylbenzenemethanol	$C_8H_{10}O$	123.0800	122.0732	M+H	589-18-4	HMDB0041609	C06757	80.0491;105.0444;77.0383
38	Isocrotonic acid	$C_4H_6O_2$	124.9995	86.0368	M+K	503-64-0	HMDB0034439	—	69.0335
39	Pimelic acid	$C_7H_{12}O_4$	125.0590	160.0736	M+H-2H_2O	111-16-0	HMDB0000857	C02656	98.9839;80.9733
40	2-Aminoethylphosphonate	$C_2H_8NO_3P$	126.0160	125.0242	M+H	2041-14-7	HMDB0011747	C03557	98.9838;92.9697
41	Taurine	$C_2H_7NO_3S$	126.0233	125.0147	M+H	107-35-7	HMDB0000251	C00245	107.92
42	Thymine	$C_5H_6N_2O_2$	127.0503	126.0424	M+H	65-71-4	HMDB00262	C00178	109.0402
43	5-Hydroxymethyl-2-furancarboxaldehyde	$C_6H_6O_3$	127.0520	126.1100	M+H	67-47-0	HMDB0034355	—	109.02;81.01
44	Dihydrothymine	$C_5H_8N_2O_2$	129.0540	128.0586	M+H	696-04-8	HMDB0000079	C00906	112.1117;84.0805
45	Lysine	$C_6H_{14}N_2O_2$	129.0910	146.1055	M+H-H_2O	56-87-1	HMDB0000182	C00047	84.0805;70.0648
46	5-Oxoproline	$C_5H_7NO_3$	130.0490	129.0426	M+H	—	—	C01879	84.0441;113.1151
47	Indole-3-carbinol	C_9H_9NO	130.0490	147.0684	M+H-H_2O	700-06-1	HMDB0005785	—	103.0538
48	1-Aminocyclopentanecarboxylic acid	$C_6H_{11}NO_2$	130.0860	129.0790	M+H	52-52-8	HMDB0062225	C03969	85.0837;113.115
49	Hydroxyproline	$C_5H_9NO_3$	132.0650	131.0582	M+H	13504-85-3	HMDB0000725	C01157	86.0961

50	Beta-Guanidinopropionic acid	$C_4H_9N_3O_2$	132.0650	131.0695	M+H	353-09-3	HMDB0013222	C03065	86.0961;115.054
51	Acetyl-L-alanine	$C_5H_9NO_3$	132.0650	131.0582	M+H	97-69-8	HMDB0000766	—	86.0961;90.0462
52	5-Aminolevulinic acid	$C_5H_9NO_3$	132.0650	131.0582	M+H	106-60-5	HMDB0001149	C00430	86.0961;115.0539;90.0462
		$C_5H_9NO_3$	149.0930	131.0582	$M+NH_4$				
53	Creatine	$C_4H_9N_3O_2$	132.0650	131.0695	M+H	57-00-1	HMDB0000064	C00300	86.0961;115.054;90.0461
54	2-Pyrrolidinone	C_4H_7NO	132.0650	85.0528	M+HCOO+2H	616-45-5	HMDB0002039	C11118	86.0961
55	Isoleucine	$C_6H_{13}NO_2$	132.1010	131.0946	M+H	—	—	C00407	86.0961
56	Piperidine	$C_5H_{11}N$	132.1010	85.0891	M+HCOO+2H	110-89-4	HMDB0034301	C01746	86.0961;66.0566
57	Gamma-Caprolactone	$C_6H_{10}O_2$	132.1010	114.0681	$M+NH_4$	695-06-7	HMDB0003843	—	86.0961;66.0565;115.0539
58	Delta-Hexalactone	$C_6H_{10}O_2$	132.1010	114.0681	$M+NH_4$	823-22-3	HMDB0000453	—	86.0961;66.0565;115.0539
59	Leucine	$C_6H_{13}NO_2$	132.1017	131.0941	M+H	61-90-5	HMDB00687	C00123	86.0961;66.0566;115.054
60	4-Vinylguaiacol	$C_9H_{10}O_2$	133.0490	150.0681	$M+H-H_2O$	7786-61-0	HMDB0013744	C17883	91.0539;105.0444
61	Cinnamaldehyde	C_9H_8O	133.0634	132.1592	M+H	104-55-2	HMDB0003441	C00903	132.83;114.91;104.80;90.85
62	Ornithine	$C_5H_{12}N_2O_2$	133.0976	132.0894	M+H	70-26-8	HMDB0000214	C00077	115.0534
63	Ortho-Hydroxyphenylacetic acid	$C_8H_8O_3$	135.0440	152.0473	$M+H-H_2O$	611-71-2	HMDB0000669	C05852	105.0444;77.0382
64	4-Hydroxy-3-methylbenzoic acid	$C_8H_8O_3$	135.0440	152.0473	$M+H-H_2O$	50-85-1	HMDB0004815	C14103	107.0852;91.0539
65	Cinnamyl alcohol	$C_9H_{10}O$	135.0650	134.0732	M+H	104-54-1	HMDB0029698	C02394	91.0539;105.0695;119.06
66	2-Methylacetophenone	$C_9H_{10}O$	135.0807	134.0726	M+H	577-16-2	HMDB32386	—	93.0699;117.0699
67	2,4-Dimethylbenzaldehyde	$C_9H_{10}O$	135.0825	134.1751	M+H	15764-16-6	HMDB0032142	—	107.0855
68	Piperitone	$C_{10}H_{16}O$	135.1010	152.1201	$M+H-H_2O$	89-81-6	HMDB0034975	—	109.0102

69	Pulegone	$C_{10}H_{16}O$	135.1010	152.1201	M+H-H_2O	89-82-7	HMDB0035604	C09893	105.0444;92.0254;109.0104
70	Benzothiazole	C_7H_5NS	136.0219	135.1860	M+H	95-16-9	HMDB0032930	—	135.92;107.87
71	Acetylarylamine	C_8H_9NO	136.0610	135.0684	M+H	103-84-4	HMDB0001250	C07565	91.0539;107.0488;109.0103
72	Erythrono-1,4-lactone	$C_4H_6O_4$	136.0610	118.0266	M+NH_4	15667-21-7	HMDB0000349	—	119.0349;91.0539
73	Tetrahydro-2-methylthiophen-3-ol	$C_5H_{10}OS$	136.0610	118.0452	M+NH_4	149834-43-5	HMDB0035244	—	119.0349;91.0539
74	2-Phenylacetamide	C_8H_9NO	136.0610	135.0684	M+H	103-81-1	HMDB0010715	C02505	91.0539
75	Ethyl carbamate	$C_3H_7NO_2$	136.0610	89.0477	M+HCOO+2H	51-79-6	HMDB0031219	C01537	91.0539
76	4,6-Diamino-5-formamidopyrimidine	$C_5H_7N_5O$	136.0750	153.0651	M+H-H_2O	5122-36-1	HMDB0004816	C06502	119.0349;92.024;109.0104
77	2,4-diaminobutyric acid	$C_4H_{10}N_2O_2$	136.0960	118.0742	M+NH_4	1758-80-1	HMDB0006284	—	119.0349;92.024
78	Amphetamine	$C_9H_{13}N$	136.0960	135.1048	M+H	300-62-9	HMDB0014328	C07514	119.0348;91.0539
79	3-Phenylpropylamine	$C_9H_{13}N$	136.0960	135.1048	M+H	582-22-9	HMDB0245973	—	119.0349;91.0539;107.0488
80	4-Fluoroamphetamine	$C_9H_{12}FN$	136.0960	153.0954	M+H-H_2O	1626-71-7	HMDB0246424	—	91.0539;109.0103
81	6-Methylnicotinamide	$C_7H_8N_2O$	137.0590	136.0637	M+H	6960-22-1	HMDB0013704	—	92.0492;78.0335;96.0441
82	Benzamideoxime	$C_7H_8N_2O$	137.0707	136.0637	M+H	613-92-3	HMDB0248971	—	78.0335
83	2-Methoxybenzaldehyde	$C_8H_8O_2$	137.0707	136.0524	M+H	135-02-4	HMDB0033766	—	94.0648;92.0492;78.0335
84	Phenyl isocyanate	C_7H_5NO	137.0707	119.0371	M+NH_4	103-71-9	HMDB0062270	—	94.0648;92.0492
85	2,3-Butanediol	$C_4H_{10}O_2$	137.0708	90.0681	M+HCOO+2H	513-85-9	HMDB0003156	C03044	92.0491
86	2-Aminobenzamide	$C_7H_8N_2O$	137.0708	136.0637	M+H	88-68-6	HMDB0033947	—	94.0648;119.0349
87	3-Aminobenzamide	$C_7H_8N_2O$	137.0710	136.0637	M+H	3544-24-9	HMDB0245814	—	94.0648;92.0492;78.0335

88	Geraniol	$C_{10}H_{18}O$	137.1320	154.1358	M+H-H_2O	106-24-1	HMDB0035155	C01500	92.0492
89	Aniline	C_6H_7N	138.0310	93.0578	M-H+2Na	100849-37-4	—	C00292	95.0682;93.0525;66.0565
90	Trigonelline	$C_7H_7NO_2$	138.0520	137.0477	M+H	535-83-1	HMDB0000875	C01004	93.0525
91	2-Hydroxypyridine	C_5H_5NO	142.0470	95.0371	M+HCOO+2H	142-08-5	HMDB0013751	C02502	66.0565;96.0442
92	Clomethiazole	C_6H_8ClNS	144.0050	161.0066	M+H-H_2O	1867-58-9	—	D07330	84.0805;113.0291;126.0369
93	Stachydrine	$C_7H_{13}NO_2$	144.1010	143.0946	M+H	471-87-4	HMDB0004827	C10172	84.0805
94	Methyl aminolevulinate	$C_6H_{11}NO_3$	146.0810	145.0739	M+H	33320-16-0	HMDB0015127	D08204	117.057;84.0804;72.0805
95	Spermidine	$C_7H_{19}N_3$	146.1650	145.1579	M+H	—	—	C00315	117.057;72.0805;84.0805
96	Vigabatrin	$C_6H_{11}NO_2$	147.1010	129.0790	M+NH_4	60643-86-9	HMDB0015212	C07500	66.0564
97	Cis-Jasmone	$C_{11}H_{16}O$	147.1010	164.1201	M+H-H_2O	488-10-8	HMDB0035601	C08490	91.0539;66.0565;105.0443
98	Ethylglycine	$C_4H_9NO_2$	148.0790	103.0633	M-H+2Na	627-01-0	HMDB0041945	—	84.0441
99	N,N-Dimethylhistidine	$C_8H_{13}N_3O_2$	148.0960	183.1008	M+H-2H_2O	24940-57-6	—	C04259	121.0393;66.0564
100	3,4-Dihydroxymandelic acid	$C_8H_8O_5$	149.0230	184.0372	M+H-2H_2O	775-01-9	HMDB0001866	C05580	121.0392
101	Ethylparaben	$C_9H_{10}O_3$	149.0440	166.0630	M+H-H_2O	120-47-8	HMDB0032573	D01647	121.0283
102	Dihydrojasmone	$C_{11}H_{18}O$	149.1320	166.1358	M+H-H_2O	1128-08-1	HMDB0031565	—	111.0438;93.0332;105.0444
103	Methionine	$C_5H_{11}NO_2S$	150.0589	149.0510	M+H	63-68-3	HMDB0000696	C00073	104.0712;133.0323
104	(-)-Carvone	$C_{10}H_{14}O$	151.0960	150.1045	M+H	6485-40-1	HMDB0035089	C01767	66.0564;79.0539;93.0696
105	10-Hydroxy-2-decenoic acid	$C_{10}H_{18}O_3$	151.0960	186.1256	M+H-2H_2O	765-01-5	HMDB0244269	—	123.0324;95.0853
106	(2-Furoyl)glycine	$C_7H_7NO_4$	152.0230	169.0375	M+H-H_2O	5657-19-2	HMDB0000439	—	124.0241;66.0565
107	Guanine	$C_5H_5N_5O$	152.0568	151.0494	M+H	73-40-5	HMDB0000132	C00242	110.0354;135.0307

108	2-(Methylamino)benzoic acid	$C_8H_9NO_2$	152.0700	151.0633	M+H	119-68-6	HMDB0032609	C03005	134.0597;66.0565
109	Diethyl phosphate	$C_4H_{11}O_4P$	155.1060	154.0395	M+H	598-02-7	HMDB0012209	C06608	98.9838;113.0083;92.9674
110	Histidine	$C_6H_9N_3O_2$	156.0760	155.0695	M+H	71-00-1	HMDB0000177	C00135	110.0709;83.0601;93.0444
111	4,6-Dioxoheptanoic acid	$C_7H_{10}O_4$	159.0650	158.0579	M+H	51568-18-4	HMDB0000635	—	113.008;130.0647
112	2-Phenyl-4-pentenal	$C_{11}H_{12}O$	161.0964	160.0888	M+H	24401-36-3	HMDB0035207	—	53.0386;79.0542;91.0542
113	Bethanechol	$C_7H_{16}N_2O_2$	161.1170	160.1212	M+H	674-38-4	HMDB0015154	C06850	119.0852
114	2-Amino-2-deoxymannose	$C_6H_{13}NO_5$	162.0760	179.0794	M+H-H_2O	14307-02-9	—	C03570	103.0386;85.0281;66.0561
115	Carnitine	$C_7H_{16}NO_3$	162.1121	162.1130	M+H	541-15-1	HMDB0000062	C00318	85.0284;103.039
116	Cassiastearoptene	$C_{10}H_{10}O_2$	163.0750	162.0681	M+H	1504-74-1	HMDB0033830	—	105.0443;77.0382;92.0253
117	N,N-Dimethylaniline	$C_8H_{11}N$	163.1070	121.0891	M+CH_3CN+H	121-69-7	HMDB0001020	C02846	105.0443;77.0382;92.0253
118	4-Guanidinobutyric acid	$C_5H_{11}N_3O_2$	163.1320	145.0851	M+NH_4	13890-14-7	HMDB0003464	C01035	70.0649;62.9288;80.0492
119	Benzenebutanoic acid	$C_{10}H_{12}O_2$	165.0903	164.0837	M+H	1821-12-1	HMDB0000543	—	146.93;136.92;122.88
		$C_{10}H_{12}O_2$	228.1010	164.0837	M+CH_3CN+Na				
120	Ethenzamide	$C_9H_{11}NO_2$	166.0710	165.0790	M+H	938-73-8	—	D01466	120.0804;103.0539;107.0488
121	Pholedrine	$C_{10}H_{15}NO$	166.1230	165.1154	M+H	370-14-9	HMDB0060767	D08370	120.0804;107.0488;93.0695
122	Hordenine	$C_{10}H_{15}NO$	166.1230	165.1154	M+H	539-15-1	HMDB0004366	C06199	103.0539;93.0696;91.0539
123	Erythrose	$C_4H_8O_4$	167.0550	120.0423	M+HCOO+2H	1758-51-6	HMDB0250746	—	121.0281
124	3-Methylxanthine	$C_6H_6N_4O_2$	167.0550	166.0491	M+H	1076-22-8	HMDB0001886	C16357	121.0394;148.9594
125	4-Hydroxymandelonitrile	$C_8H_7NO_2$	167.0890	149.0477	M+NH_4	—	—	C00650	104.0572;64.9269;121.0394
126	Phthalic acid	$C_8H_6O_4$	167.1430	166.0266	M+H	88-99-3	HMDB0002107	C01606	121.0394

127	Norepinephrine	$C_8H_{11}NO_3$	170.0810	169.0739	M+H	51-41-2	HMDB0037685	C00547	64.9269;134.0597;72.3879
128	Camphor	$C_{10}H_{16}O$	170.1540	152.1201	$M+NH_4$	76-22-2	HMDB0059838	C18369	66.0553
129	Juglone	$C_{10}H_6O_3$	175.0360	174.0317	M+H	481-39-0	HMDB0030773	C03840	91.0539;66.0561;105.0696
130	Arginine	$C_6H_{14}N_4O_2$	175.1193	174.1117	M+H	74-79-3	HMDB0000517	C00062	70.0664;116.0718;130.0991
131	Acetyl-L-aspartic acid	$C_6H_9NO_5$	176.0550	175.0481	M+H	997-55-7	HMDB0000812	C01042	70.0648;133.0646
132	High Proline	$C_6H_{11}NO_2$	176.0910	129.0790	M+HCOO+2H	56879-46-0	HMDB29444	—	66.0561;70.0648
133	4,6,8-Megastigmatriene	$C_{13}H_{20}$	177.1642	176.1565	M+H	51468-86-1	HMDB0035180	—	81.0699;93.0699;107.0855
134	Norleucine	$C_6H_{13}NO_2$	178.1070	131.0946	M+HCOO+2H	1319-82-0	HMDB01645	C01933	120.9818;109.9658;86.0961
135	6-Deoxyfagomine	$C_6H_{13}NO_2$	178.1070	131.0946	M+HCOO+2H	197449-09-5	HMDB0036382	—	86.0961
136	Alpha-Terpineol acetate	$C_{12}H_{20}O_2$	179.1430	196.1463	$M+H-H_2O$	80-26-2	HMDB0032051	C12300	66.0564
137	Beta-D-Glucosamine	$C_6H_{13}NO_5$	180.0860	179.0794	M+H	14257-69-3	HMDB0030091	C08349	107.0726;120.0805
138	Mexiletine	$C_{11}H_{17}NO$	180.1380	179.1310	M+H	180966-61-4	HMDB0014523	C07220	120.0806;107.0727
139	Methylephedrine	$C_{11}H_{17}NO$	180.1380	179.1310	M+H	552-79-4	HMDB0041932	—	107.0726
140	Picolinoylglycine	$C_8H_8N_2O_3$	181.0620	180.0535	M+H	5616-29-5	HMDB0059766	—	153.0694;66.0564;107.06
141	P-Mentha-1,3,8-triene	$C_{10}H_{14}$	181.1220	134.1096	M+HCOO+2H	18368-95-1	HMDB0037013	—	66.0564;135.0549;107.06
142	5-Hydroxymethyluracil	$C_5H_6N_2O_3$	184.0730	142.0378	$M+CH_3CN+H$	4433-40-3	HMDB0000469	C03088	124.9995;98.9839
143	6-Methylmercaptopurine	$C_6H_6N_4S$	184.0730	166.0313	$M+NH_4$	133762-85-3	HMDB0060412	C16614	124.9995;71.0726;98.9839
144	Phosphorylcholine	$C_5H_{15}NO_4P$	184.0736	184.0739	M+H	3616-04-4	HMDB0001565	C00588	60.0808;86.0972;98.9791
145	Methyprylon	$C_{10}H_{17}NO_2$	184.1330	183.1259	M+H	125-64-4	HMDB0015239	D01150	124.9995;86.0962;98.9839
146	Val-Cys	$C_8H_{16}N_2O_3S$	185.0940	220.0882	$M+H-2H_2O$	—	HMDB0029124	—	105.1099

147	Triethylenetetramine	$C_6H_{18}N_4$	185.1170	146.1531	M+K	112-24-3	—	C07166	87.0994;98.9838
148	Acetylcysteine	$C_5H_9NO_3S$	186.0080	163.0303	M+Na	616-91-1	HMDB0001890	C06809	140.0015;86.0961;66.0564
149	6-Hydroxynicotinic acid	$C_6H_5NO_3$	186.0160	139.0269	M+HCOO+2H	15864-85-4	HMDB0002658	C01020	140.0015;86.0961;66.0565
150	4-Hydroxycyclohexylcarboxylic acid	$C_7H_{12}O_3$	186.1120	144.0786	M+CH_3CN+H	3685-26-5	HMDB0001988	—	127.0037;66.0564;144.3115
151	5-(2-Hydroxyethyl)-4-methylthiazole	C_6H_9NOS	188.0140	143.0405	M-H+2Na	137-00-8	HMDB0032985	C04294	144.0804
152	5-Methoxyindole-3-acetic acid	$C_{11}H_{11}NO_3$	188.0680	205.0739	M+H-H_2O	3471-31-6	HMDB0004096	C05660	118.0648;146.0597;144.0804
153	N8-Acetylspermidine	$C_9H_{23}N_3O$	188.1640	189.1841	M+H	34450-15-2	HMDB0002189	C01029	146.0596;144.0804
154	Diaminopimelic acid	$C_7H_{14}N_2O_4$	191.1040	190.0954	M+H	583-93-7	HMDB0001370	—	116.9507
155	Megastigmatrienone	$C_{13}H_{18}O$	191.1270	190.1358	M+H	—	HMDB0059906	—	160.018;149.0132;109.966
156	Spermine	$C_{10}H_{26}N_4$	203.2230	202.2157	M+H	71-44-3	HMDB0001256	C00750	84.0805;112.1119
157	Acetylcarnitine	$C_9H_{18}NO_4$	204.1239	203.1158	M+H	3040-38-8	HMDB0000201	C02571	85.0284;145.0495
158	Tetrahydro-L-biopterin	$C_9H_{15}N_5O_3$	206.1000	241.1175	M+H-2H_2O	69056-38-8	HMDB0000027	C00272	96.0805;62.9288;109.9659
159	Betonicine	$C_7H_{13}NO_3$	206.1000	159.0895	M+HCOO+2H	515-25-3	HMDB0029412	C08269	96.0805;83.0601;91.9554
160	Pregabalin	$C_8H_{17}NO_2$	206.1380	159.1259	M+HCOO+2H	148553-50-8	HMDB0014375	D02716	96.0805;83.0601
161	1-Methylguanine	$C_6H_7N_5O$	207.0980	165.0651	M+CH_3CN+H	938-85-2	HMDB0003282	C04152	137.0081
162	3-Amino-2-methylpropanoic acid	$C_4H_9NO_2$	207.1350	103.0633	2M+H	144-90-1	HMDB0003911	C05145	75.0258
163	Phosphoserine	$C_3H_8NO_6P$	207.9980	185.0089	M+Na	1446756-47-3	HMDB0000272	C01005	64.927;109.966;96.0806
164	Aminocaproic acid	$C_6H_{13}NO_2$	207.9980	131.0946	M-H+2K	60-32-2	HMDB0001901	C02378	64.927;96.0806;70.0649
165	Genipin	$C_{11}H_{14}O_5$	209.0770	226.0841	M+H-H_2O	6902-77-8	HMDB0035830	C09780	64.9269;97.0837;138.9873

166	Kynurenine	$C_{10}H_{12}N_2O_3$	209.0770	208.0848	M+H	2922-83-0	HMDB0000684	C00328	64.927;135.9815;165.0698
167	Jasmonic acid	$C_{12}H_{18}O_3$	211.1330	210.1256	M+H	6894-38-8	HMDB0032797	C08491	192.9801;152.0129
168	Isoprenaline	$C_{11}H_{17}NO_3$	212.1280	211.1208	M+H	7683-59-2	HMDB0015197	C07056	165.9746;137.98;135.9817
169	Gabapentin	$C_9H_{17}NO_2$	218.1380	171.1259	M+HCOO+2H	360-70-3	HMDB0005015	C07018	171.9928
170	Allocystathionine	$C_7H_{14}N_2O_4S$	223.0630	222.0674	M+H	535-34-2	HMDB0000455	C00542	192.0461;209.0113;207.0321
171	Gly-Phe	$C_{11}H_{14}N_2O_3$	223.0960	222.1004	M+H	3321/3/7	HMDB0028848	—	207.0321;178.0304
172	Canavanine	$C_5H_{12}N_4O_3$	223.0960	176.0909	M+HCOO+2H	543-38-4	HMDB0002706	C00308	178.0307
173	Acetyl-L-tyrosine	$C_{11}H_{13}NO_4$	224.0919	223.0845	M+H	537-55-3	HMDB0000866	C01657	165.0552;206.0817
174	2-Amino-2-methyl-1,3-propanediol	$C_4H_{11}NO_2$	228.1950	105.0790	$2M+NH_4$	115-69-5	—	C11260	88.0754
175	Ergothioneine	$C_9H_{15}N_3O_2S$	230.1030	229.0885	M+H	497-30-3	HMDB0003045	C05570	85.1009;66.0549
176	Benzaldehyde	C_7H_6O	230.1030	106.0419	$2M+NH_4$	100-52-7	HMDB0006115	C00193	66.0549
177	Pyridoxal phosphate	$C_8H_{10}NO_6P$	230.1380	247.0246	$M+H-H_2O$	54-47-7	HMDB0001491	C00018	66.0549
178	Diethyl phthalic acid	$C_{12}H_{14}O_4$	245.0760	222.0892	M+Na	68988-18-1	HMDB0094660	C14175	151.0114;163.0288
179	Carnitine 2-methyl-C4	$C_{12}H_{23}NO_4$	246.1690	245.1627	M+H	31023-25-3	HMDB0000378	—	85.0281
180	Myristic acid	$C_{14}H_{28}O_2$	246.2430	228.2089	$M+NH_4$	544-63-8	HMDB0000806	C06424	229.2168
181	Ser-Lys	$C_9H_{19}N_3O_4$	256.1210	233.1376	M+Na	22677-61-8	HMDB0029044	—	102.091;88.0754;70.0648
182	Hexadecanamide/Palmitic amide	$C_{16}H_{33}NO$	256.2609	255.4393	M+H	629-54-9	HMDB0012273	—	101.92;87.89
183	Glu-Gln	$C_{10}H_{17}N_3O_6$	258.1000	275.1117	$M+H-H_2O$	—	HMDB0011738	C05283	102.0911;184.0731
184	Benzamidine	$C_7H_8N_2$	258.1690	120.0687	$2M+NH_4$	618-39-3	HMDB0248970	C01784	104.1067
185	Pantothenate	$C_9H_{17}NO_5$	264.0790	219.1107	M-H+2Na	79-83-4	HMDB0000210	C00864	66.0541;189.0447;92.9736

186	Thiamine	$C_{12}H_{17}N_4OS$	265.1109	265.1123	M+H	70-16-6	HMDB0000235	C00378	144.0483
187	Acetyl-N-formyl-5-methoxykynurenamine	$C_{13}H_{16}N_2O_4$	265.1110	264.1110	M+H	52450-38-1	HMDB0004259	C05642	232.0867;189.0446
188	Glycerophosphocholine	$C_8H_{20}NO_6P$	280.0910	257.1028	M+Na	—	HMDB0000086	—	104.1068;86.0962
189	Alloisoleucine	$C_6H_{13}NO_2$	280.2270	131.0946	2M+NH_4	1509-34-8	HMDB0000557	C21096	104.1068;73.0466
190	Oleamide	$C_{18}H_{35}NO$	282.2796	281.2719	M+H	301-02-0	HMDB02117	C19670	83.0855;97.1012
191	Alanyllysine	$C_9H_{19}N_3O_3$	284.0980	217.1426	M-2H+3Na	6366-77-4	HMDB0028692	—	102.0912;88.0755
192	Prolyl-Tryptophan	$C_{16}H_{19}N_3O_3$	284.1330	301.1426	M+H-H_2O	35310-39-5	HMDB0029028	—	102.0911;66.0538;70.0648
193	Vitamin A	$C_{20}H_{30}O$	287.2375	286.2297	M+H	68-26-8	HMDB0000305	D00069	269.2264
194	Muramic acid	$C_9H_{17}NO_7$	296.0665	251.1005	M-H+2Na	1114-41-6	—	C06470	105.1101;
195	5'-Methylthioadenosine	$C_{11}H_{15}N_5O_3S$	298.0965	297.0896	M+H	2457-80-9	HMDB0001173	C00170	136.0616;104.1068;75.0261
196	Methylimidazoleacetic acid	$C_6H_8N_2O_2$	298.1490	140.0586	2M+NH_4	2625-49-2	HMDB0002820	C05828	75.0261;97.0282
197	Sphingosine	$C_{18}H_{37}NO_2$	300.2885	299.4919	M+H	123-78-4	HMDB0000252	C00319	282.22;256.21;238.27;212.21
198	Palmitoyl ethanolamide	$C_{18}H_{37}NO_2$	300.2901	299.2824	M+H	544-31-0	HMDB0002100	C16512	239.2369;282.2791
199	Sphinganine	$C_{18}H_{39}NO_2$	302.3059	301.2981	M+H	764-22-7	HMDB0000269	C00836	284.2973
200	11,12-EET	$C_{20}H_{32}O_3$	303.2306	320.4730	M+H-H2O	—	HMDB0244445	C14770	166.84;149.00
201	Oleoylethanolamide	$C_{20}H_{39}NO_2$	308.2957	325.2981	M+H-H_2O	111-58-0	HMDB0002088	C20792	265.2526
202	MG(16:0)	$C_{19}H_{38}O_4$	313.2743	330.2770	M+H-H_2O	—	HMDB0011564	—	81.0522
203	Phytosphingosine	$C_{18}H_{39}NO_3$	318.3007	317.2930	M+H	554-62-1	HMDB0004610	C12144	282.2797;300.2903
204	Guanosine	$C_{10}H_{13}N_5O_5$	322.0551	283.0917	M+K	118-00-3	HMDB0000133	—	151.0489

205	MG(0:0/15:0/0:0)	$C_{18}H_{36}O_4$	334.2957	316.2614	$M+NH_4$	—	—	—	299.2581;317.2686
206	3-Methyl-5-pentyl-2-furanundecanoate	$C_{21}H_{36}O_3$	337.2737	336.2664	M+H	57818-37-8	HMDB0031005	—	151.1117;319.2632
207	Adenosine 2'-phosphate	$C_{10}H_{14}N_5O_7P$	348.0712	347.0631	M+H	130-49-4	HMDB0011617	C00946	136.0618
208	MG(0:0/i-17:0/0:0)	$C_{20}H_{40}O_4$	362.3271	344.2927	$M+NH_4$	—	—	—	344.3159
209	Lithocholic acid	$C_{24}H_{40}O_3$	415.2602	376.2977	M+K	434-13-9	HMDB0000761	C03990	119.0855
210	Lysopc 16:0	$C_{24}H_{50}NO_7P$	496.3390	495.3325	M+H	17364-16-8	HMDB0010382	—	184.0733;478.3289;313.2737
211	LPC(16:0)	$C_{24}H_{50}NO_7P$	496.3401	495.3325	M+H	—	—	—	184.0731
212	LPC(18:1)	$C_{26}H_{52}NO_7P$	522.3555	521.3481	M+H	—	—	—	184.0729
213	LPC(18:0)	$C_{26}H_{54}NO_7P$	524.3720	523.3638	M+H	—	—	—	184.0728
214	DG(32:1)	$C_{35}H_{66}O_5$	549.4890	566.4910	$M+H-H_2O$	—	HMDB0007211	—	285.2424;339.2894
215	Ceramide	$C_{42}H_{81}NO_3$	648.6310	647.6216	M+H	—	HMDB0004953	—	264.2686;630.6183
216	PC(28:0)	$C_{36}H_{72}NO_8P$	678.5078	677.4996	M+H	—	HMDB0007866	—	184.0729
217	PC(29:1)	$C_{37}H_{72}NO_8P$	690.5071	689.4996	M+H	—	—	—	184.0731
218	PC(29:0)	$C_{37}H_{74}NO_8P$	692.5236	691.5152	M+H	—	—	—	184.0728
219	PC(30:1)	$C_{38}H_{74}NO_8P$	704.5239	703.5152	M+H	—	—	—	184.0728
220	PC(30:0)	$C_{38}H_{76}NO_8P$	706.5397	705.5309	M+H	—	—	—	184.0731
221	PC(31:1)	$C_{39}H_{76}NO_8P$	718.5396	717.5309	M+H	—	—	—	184.0731
222	DG(44:9)	$C_{47}H_{74}O_5$	718.5758	718.5536	$M+NH_4-H_2O$	—	—	—	701.5503
223	PC(31:0)	$C_{39}H_{78}NO_8P$	720.5561	719.5465	M+H	—	—	—	184.0728
224	PC(32:1)	$C_{40}H_{78}NO_8P$	732.5553	731.5465	M+H	—	—	—	184.0739

225	PC(32:0)	$C_{40}H_{80}NO_8P$	734.5710	733.5621	M+H	—	—	—	184.0728
226	PC(33:3)	$C_{41}H_{76}NO_8P$	742.5402	741.5308	M+H	—	—	—	184.0731
227	PC(33:2)	$C_{41}H_{78}NO_8P$	744.5554	743.5465	M+H	—	—	—	184.0728
228	PC(34:0)	$C_{42}H_{84}NO_8P$	744.5920	761.5934	M+H-H_2O	—	—	—	184.0728
229	PC(33:1)	$C_{41}H_{80}NO_8P$	746.5713	745.5622	M+H	—	—	—	184.0729
230	PC(34:1)	$C_{42}H_{82}NO_8P$	760.5862	759.5778	M+H	—	—	—	184.0729
231	PC(35:5)	$C_{43}H_{76}NO_8P$	766.5391	765.5309	M+H	—	—	—	184.0728
232	PC(36:4)	$C_{43}H_{78}NO_8P$	768.5908	767.5465	M+H	—	—	—	184.0729
233	PC(35:3)	$C_{43}H_{80}NO_8P$	770.5714	769.5621	M+H	—	—	—	184.0731
234	PC(35:2)	$C_{43}H_{82}NO_8P$	772.5867	771.5778	M+H	—	—	—	184.0729
235	PC(35:1)	$C_{43}H_{84}NO_8P$	774.6024	773.5935	M+H	—	—	—	184.0728
236	PC(36:5)	$C_{44}H_{78}NO_8P$	780.5547	779.5465	M+H	—	—	—	184.0731
237	PC(36:3)	$C_{44}H_{82}NO_8P$	784.5870	783.5778	M+H	—	—	—	184.0727
238	PC(36:2)	$C_{44}H_{84}NO_8P$	786.6021	785.5935	M+H	—	—	—	184.0730
239	PC(34:2)	$C_{42}H_{80}NO_8P$	796.5260	757.5622	M+K	—	—	—	184.0733
240	PC(37:2)	$C_{45}H_{86}NO_8P$	800.6172	799.6091	M+H	—	—	—	184.0729
241	PC(38:7)	$C_{46}H_{78}NO_8P$	804.5530	803.5465	M+H	—	—	—	184.0729
242	PC(38:6)	$C_{46}H_{80}NO_8P$	806.5719	805.5622	M+H	—	—	—	184.0728
243	PC(38:5)	$C_{46}H_{82}NO_8P$	808.5868	807.5778	M+H	—	—	—	184.0729
244	PC(36:1)	$C_{44}H_{86}NO_8P$	810.6027	787.6091	M+Na	—	—	—	627.5323;751.5248

245	PC(38:3)	$C_{27}H_{44}O_3$	812.6190	811.6091	M+H	—	—	—	629.5503
246	PC(38:2)	$C_{46}H_{88}NO_8P$	814.6330	813.6248	M+H	—	—	—	184.0728
247	PC(40:7)	$C_{48}H_{82}NO_8P$	832.5866	831.5778	M+H	—	—	—	184.0728
248	PC(40:6)	$C_{48}H_{84}NO_8P$	834.6016	833.5935	M+H	—	—	—	184.0731
249	PC(40:5)	$C_{48}H_{86}NO_8P$	836.6206	835.6091	M+H	—	—	—	184.0729
Negative ion mode									
NO.	**Metabolites**	**Formula**	**Precursor**	**Mass**	**Ions**	**CAS_ID**	**HMDB_ID**	**KEGG_ID**	**MS/MS fragments**
250	2-Oxobutanoic acid	$C_4H_6O_3$	101.0245	102.0317	M-H	600-18-0	HMDB0000005	C00109	83.0139
251	Serine	$C_3H_7NO_3$	104.0360	105.0426	M-H	302-84-1	HMDB0000187	C00065	74.0248;58.8439
252	P-Cresol	C_7H_8O	107.0500	108.0575	M-H	106-44-5	HMDB0001858	C01468	79.9574;66.0735;92.9932
253	Butyric acid	$C_4H_8O_2$	109.0300	88.0524	M+Na-2H	107-92-6	HMDB0000039	C00246	60.9470;81.9534;53.9918
254	Pyrrole-2-carboxylic acid	$C_5H_5NO_2$	110.0250	111.0320	M-H	634-97-9	HMDB0004230	C05942	66.0734;80.0381
255	3-Furancarboxylic acid	$C_5H_4O_3$	111.0090	112.0160	M-H	488-93-7	HMDB0000444	C00106	78.9592;66.0734;72.4084
256	2,4-Hexadienoic acid	$C_6H_8O_2$	111.0450	112.0524	M-H	110-44-1	HMDB0029581	D05892	66.0734;94.6238
257	Creatinine	$C_4H_7N_3O$	112.0410	113.0589	M-H	60-27-5	HMDB0000562	C00791	68.1633
258	Glutaric acid	$C_5H_8O_4$	113.0250	132.0423	M-H_2O-H	110-94-1	HMDB0000661	C00489	68.9959;79.9563
259	2-Methyl-3-pentenoic acid	$C_6H_{10}O_2$	113.0610	114.0681	M-H	1879-03-4	—	—	68.9959;66.0734;
260	Iminodiacetic acid	$C_4H_7NO_4$	114.0200	133.0375	M-H_2O-H	142-73-4	HMDB0011753	C19911	68.7729;71.7443;58.8481
261	Malic acid	$C_4H_6O_5$	115.0040	134.0215	M-H_2O-H	6915-15-7	HMDB0000744	C00711	72.4083

262	2,3-Dihydroxy-isovalerate	$C_5H_{10}O_4$	115.0400	134.0579	M-H_2O-H	19451-56-0	HMDB0012141	C04039	72.4083
263	Hexanoic acid	$C_6H_{12}O_2$	115.0770	116.0837	M-H	—	—	C01585	72.4083
264	Methylmalonic acid	$C_4H_6O_4$	117.0200	118.0266	M-H	516-05-2	HMDB0000202	C02170	72.4084;69.1319
265	Salicylamide	$C_7H_7NO_2$	118.0300	137.0477	M-H_2O-H	65-45-2	HMDB0015687	D01811	66.0735;90.0350.
266	Allo-threonine	$C_4H_9NO_3$	118.0510	119.0582	M-H	144-98-9	—	C05519	74.0248
267	Threonine	$C_4H_9NO_3$	118.0510	119.0582	M-H	13095-55-1	HMDB0000167	C00188	74.0248
268	4-Methylbenzaldehyde	C_8H_8O	119.0500	120.0575	M-H	104-87-0	HMDB0029638	C06758	93.0346;74.4223
269	4-hydroxystyrene	C_8H_8O	119.0500	120.0575	M-H	2628-17-3	HMDB0004072	C05627	66.0735;93.0346;51.7171
270	Benzoic acid	$C_7H_6O_2$	121.0300	122.0368	M-H	65-85-0	HMDB0001870	C00180	92.9933
271	3-Hydroxybenzaldehyde	$C_7H_6O_2$	121.0300	122.0368	M-H	100-83-4	—	C03067	92.0268;66.0734;51.2414
272	Maltol	$C_6H_6O_3$	125.0250	126.0317	M-H	118-71-8	HMDB0030776	C11918	79.9575;66.0734
273	1H-Imidazol-1-ylacetic acid	$C_5H_6N_2O_2$	125.0250	126.0429	M-H	22884-10-2	HMDB0029736	—	80.9617
274	1,2,3-Trihydroxybenzene	$C_6H_6O_3$	125.0250	126.0317	M-H	87-66-1	HMDB0013674	C01108	79.9574;;66.0734
275	2-methyl-1,3-Cyclohexanedione	$C_7H_{10}O_2$	125.0610	126.0681	M-H	1193-55-1	HMDB0034080	—	79.9574;66.0734
276	Adipic acid	$C_6H_{10}O_4$	127.0400	146.0579	M-H_2O-H	124-04-9	HMDB0000448	C06104	81.9532
277	Cyclohexanecarboxylic acid	$C_7H_{12}O_2$	127.0770	128.0837	M-H	98-89-5	HMDB0031342	C09822	66.0734;81.9533
278	Pyroglutamic acid	$C_5H_7NO_3$	128.0354	129.0426	M-H	149-87-1	HMDB0000805	—	72.4077
279	Hydroxyisocaproic acid	$C_6H_{12}O_3$	131.0720	132.0786	M-H	13748-90-8	HMDB0000746	—	72.4078;67.4077
280	2-Ethyl-2-Hydroxybutyric acid	$C_6H_{12}O_3$	131.0720	132.0786	M-H	3639-21-2	HMDB0001975	—	56.1665
281	Maleic acid	$C_4H_4O_4$	132.0300	116.0110	M+NH_4-2H	110-16-7	HMDB0000176	C01384	95.3789;99.4189;51.3834

282	Adenine	$C_5H_5N_5$	134.0470	135.0545	M-H	134434-49-4	HMDB0000034	C00147	107.0363;92.0254
283	4-Oxopentanoate	$C_5H_8O_3$	135.0450	116.0473	M+F	123-76-2	HMDB0000720	—	75.0088;72.4078;60.9468
284	4-Hydroxybenzoic acid	$C_7H_6O_3$	137.0240	138.0317	M-H	99-96-7	HMDB0000500	C00156	93.0458;78.9590
285	2,5-Dihydroxybenzaldehyde	$C_7H_6O_3$	137.0240	138.0317	M-H	1194-98-5	HMDB0004062	C05585	66.0733;78.9591;96.8327
286	2-(4-Hydroxyphenyl)ethanol	$C_8H_{10}O_2$	137.0610	138.0681	M-H	2380-91-8	—	C13638	66.0732;93.0346
287	4-Nitrophenol	$C_6H_5NO_3$	138.0200	139.0269	M-H	100-02-7	HMDB0001232	C00870	108.0455;66.0732;94.0299
288	2-Aminoethyl dihydrogen phosphate	$C_2H_8NO_4P$	140.0120	141.0191	M-H	1071-23-4	HMDB0000224	C00346	78.9591
289	Daminozide	$C_6H_{12}N_2O_3$	141.0560	160.0848	M-H_2O-H	1596-84-5	—	C10996	58.7564;100.8584;108.0046
290	Ectoine	$C_6H_{10}N_2O_2$	141.0560	142.0742	M-H	96702-03-3	—	C06231	84.1901;75.3660;102.1730
291	4-Hydroxyvalproic acid	$C_8H_{16}O_3$	141.0920	160.1099	M-H_2O-H	60113-82-8	HMDB0013900	C16649	66.0732;114.5427
292	Trimethadione	$C_6H_9NO_3$	142.0510	143.0582	M-H	—	HMDB0014491	D00392	60.9468
293	Indole-3-carboxaldehyde	C_9H_7NO	144.0460	145.0528	M-H	487-89-8	HMDB0029737	C08493	66.0732;51.0292;60.9468
294	4-Hydroxyquinoline	C_9H_7NO	144.0460	145.0528	M-H	611-36-9	—	C06343	66.0732;72.4076;95.3761
295	Glutamine	$C_5H_{10}N_2O_3$	145.0510	146.0691	M-H	56-85-9	HMDB0000641	C00064	66.0733;84.0454;127.0511
296	2-Methylglutaric acid	$C_6H_{10}O_4$	145.0510	146.0579	M-H	617-62-9	HMDB0000422	—	84.0454;74.0248
297	Isatin	$C_8H_5NO_2$	146.0250	147.0320	M-H	91-56-5	HMDB0061933	C11129	66.0732;92.9935;69.6941
298	Glutamic acid	$C_5H_9NO_4$	146.0460	147.0532	M-H	56-86-0	HMDB0000148	C00025	119.0502;101.0244;85.0295
		$C_5H_9NO_4$	163.0760	147.0532	M+NH_4-2H				
299	Tartaric acid	$C_4H_6O_6$	149.0100	150.0164	M-H	147-71-7	HMDB0029878	C02107	72.4077

300	4-Coumaryl alcohol	$C_9H_{10}O_2$	149.0610	150.0681	M-H	3690/5/9	HMDB03654	C02646	102.7635;51.3836
301	3-Hydroxyanthranilic acid	$C_7H_7NO_3$	152.0350	153.0426	M-H	548-93-6	HMDB0001476	C00632	108.0454
302	3-Amino-4-Hydroxybenzoic acid	$C_7H_7NO_3$	152.0350	153.0426	M-H	570-23-0	HMDB0001972	—	66.0732;79.9575
303	Linalool	$C_{10}H_{18}O$	153.1290	154.1358	M-H	126-90-9	HMDB0036101	C11389	66.0732;97.0407;81.0459
304	2-Deoxy-D-ribose	$C_5H_{10}O_4$	155.0350	134.0579	M+Na-2H	533-67-5	HMDB0245099	—	94.0492
305	Shikimic acid	$C_7H_{10}O_5$	155.0350	174.0528	M-H_2O-H	138-59-0	HMDB0003070	C00493	94.0492;138.0389;78.9591
306	Dihydroorotic acid	$C_5H_6N_2O_4$	157.0250	158.0328	M-H	5988-19-2	HMDB0003349	C00337	114.9887
307	Salicylic acid	$C_7H_6O_3$	157.0250	138.0317	M+F	69-72-7	HMDB0001895	C00805	113.0094
308	Ureidosuccinic acid	$C_{10}H_{16}N_2O_9S$	157.0250	340.0577	M-H_2O-H	13184-27-5	HMDB0000828	C00438	89.0245;114.9887
309	3,3-Dimethylglutaric acid	$C_7H_{12}O_4$	159.0660	160.0736	M-H	4839-46-7	HMDB0002441	—	114.9887;78.9592;66.0733
310	5-Hydroxyvalproic acid	$C_8H_{16}O_3$	159.1030	160.1099	M-H	53660-23-4	HMDB0013898	C16650	130.9836;114.9887
311	Carboxymethyl-L-cysteine	$C_5H_9NO_4S$	160.0070	179.0252	M-H_2O-H	638-23-3	HMDB0029415	D06393	86.9911;74.0249;116.0175
312	3-Hydroxy-3-methylglutaric acid	$C_6H_{10}O_5$	161.0460	162.0528	M-H	503-49-1	HMDB0000355	C03761	144.3546;129.0362;75.3499
313	Phenylalanine	$C_9H_{11}NO_2$	164.0715	165.0790	M-H	149597-92-2	HMDB0000159	C00079	147.0449;103.0553;72.0092
314	Homogentisic acid	$C_8H_8O_4$	167.0350	168.0423	M-H	451-13-8	HMDB0000130	C00544	123.0564;109.0490;66.0733
315	4-Ipomeanol	$C_9H_{12}O_3$	167.0710	168.0786	M-H	55659-41-1	HMDB0030472	—	66.0733
316	Glycerophosphoric acid	$C_3H_9O_6P$	171.0060	172.0137	M-H	17181-54-3	HMDB0002520	C02979	78.9591;96.9695
317	Carglumic acid	$C_6H_{10}N_2O_5$	171.0410	190.0590	M-H_2O-H	1188-38-1	HMDB0015673	C05829	128.0352;142.9662
318	Phenoxyacetic acid	$C_8H_8O_3$	171.0410	152.0473	M+F	122-59-8	HMDB0031609	C02181	78.9591;66.0733
319	Decanoic acid	$C_{10}H_{20}O_2$	171.1390	172.1463	M-H	334-48-5	HMDB0000511	C01571	78.9591;66.0733;96.9697

320	Suberic acid	$C_8H_{14}O_4$	173.0820	174.0892	M-H	505-48-6	HMDB0000893	C08278	131.0825;93.0346;66.0733
321	Cysteinylglycine	$C_5H_{10}N_2O_3S$	177.0340	178.0412	M-H	19246-18-5	HMDB0000078	C01419	74.0248;131.0463;99.0564
322	Acetylthreonine	$C_6H_{11}NO_4$	177.0920	161.0688	M+NH_4-2H	17093-74-2	HMDB0062557	—	74.0248;99.0563
323	Nicotinuric acid	$C_8H_8N_2O_3$	179.0460	180.0535	M-H	583-08-4	HMDB0003269	C05380	109.0407;135.0562
324	1,7-Dimethylxanthine	$C_7H_8N_4O_2$	179.0710	180.0647	M-H	611-59-6	HMDB0001860	C13747	135.0563
325	B-Hydroxycaprylic acid	$C_8H_{16}O_3$	179.1070	160.1099	M+F	14292-27-4	HMDB0001954	C20793	109.0407;135.0563;95.0251
326	Tyrosine	$C_9H_{11}NO_3$	180.0660	181.0739	M-H	55520-40-6	HMDB0000158	C00082	119.0501;163.0397;93.0346
327	P-Coumaric acid	$C_9H_8O_3$	180.0660	164.0473	M+NH_4-2H	501-98-4	HMDB0002035	C00811	119.0502;163.0398;93.0346
328	2-Hydroxycinnamic acid	$C_9H_8O_3$	180.0660	164.0473	M+NH_4-2H	614-60-8	HMDB0002641	C01772	119.0502;93.0347;66.0734
329	Mannitol	$C_6H_{14}O_6$	181.0715	182.0790	M-H	69-65-8	HMDB0000765	C00392	101.0244;71.0140;89.0244
330	Iditol	$C_6H_{14}O_6$	181.0715	182.0790	M-H	488-45-9	HMDB0011632	C01507	101.0244;71.0140;89.0245
331	Asp-Ala	$C_7H_{12}N_2O_5$	185.0570	204.0746	M-H_2O-H	13433-02-8	HMDB0028746	—	141.0668;99.0563;85.0409
332	1-Hydroxy-2-Naphthoate	$C_{11}H_8O_3$	187.0418	188.0473	M-H	86-48-6	—	C03203	115.0208;157.0312;66.0733
333	2-Amino-3-methylimidazo[4,5-f]quinoline	$C_{11}H_{10}N_4$	197.0820	198.0905	M-H	76180-96-6	HMDB0029706	C19180	169.0159;66.0734
334	Erythrose-4-phosphate	$C_4H_9O_7P$	198.9970	200.0086	M-H	585-18-2	HMDB0001321	C00279	78.9591;66.0734;125.0009
335	Fructose	$C_6H_{12}O_6$	201.0377	180.0634	M+Na-2H	57-48-7	HMDB0062538	C10906	164.6032
336	Zalcitabine	$C_9H_{13}N_3O_3$	210.0880	211.0957	M-H	7481-89-2	HMDB0015078	C07207	86.0612;107.0615
337	4-Aminohippuric acid	$C_9H_{10}N_2O_3$	210.0890	194.0691	M+NH_4-2H	61-78-9	HMDB0001867	D06890	74.0248;99.0564
338	2–Furanoic acid	$C_5H_4O_3$	223.0280	112.0160	2M-H	88-14-2	HMDB0000617	C01546	66.0734

339	Thymidine	$C_{10}H_{14}N_2O_5$	223.0760	242.0903	M-H_2O-H	50-89-5	HMDB0000273	C00214	100.0404
340	Umbelliferone	$C_9H_6O_3$	233.1540	162.0317	M-H	93-35-6	HMDB0029865	C09315	120.9547;198.5445
341	Glycyltyrosine	$C_{11}H_{14}N_2O_4$	237.0910	238.0954	M-H	658-79-7	HMDB0028853	—	106.9809
342	Tyr-Gly	$C_{11}H_{14}N_2O_4$	237.0911	238.0954	M-H	673-08-5	—	—	106.9808;193.0648
343	15(R)-hydroperoxy-EPE	$C_8H_{18}N_2O_4S$	237.0915	238.0987	M-H	7365-45-9	HMDB0062295	—	79.9575;122.9853;106.9808
344	Uridine	$C_9H_{12}N_2O_6$	243.0620	244.0695	M-H	58-96-8	HMDB0000296	C00299	110.0247
345	2-cis-Hexadecenoic acid	$C_{16}H_{30}O_2$	253.2170	254.2246	M-H	2825-68-5	HMDB0244666	—	66.0734;124.0073
346	Gamma-Glutamylglutamic acid	$C_{10}H_{16}N_2O_7$	257.0751	276.0958	M-H_2O-H	1116-22-9	HMDB0011737	C05282	127.0513;145.0617
347	Myo-Inositol 6-phosphate	$C_6H_{13}O_9P$	259.0220	260.0297	M-H	15421-51-9	HMDB0002985	C01177	78.9591;145.0981;168.0150
348	14-Methylhexadecanoic acid	$C_{17}H_{34}O_2$	269.2480	270.2559	M-H	5918-29-6	HMDB0031067	—	128.0353
349	Zidovudine	$C_{10}H_{13}N_5O_4$	288.0660	267.0968	M+Na-2H	30516-87-1	HMDB0014638	C07210	127.0512
350	Embelin	$C_{17}H_{26}O_4$	293.1760	294.1831	M-H	550-24-3	HMDB0251767	C10342	221.1539
351	Acetylglucosamine 1-Phosphate	$C_8H_{16}NO_9P$	300.0480	301.0563	M-H	6866-69-9	HMDB0001367	C04256	78.9591;144.3556;129.1032
352	Glutathione	$C_{10}H_{17}N_3O_6S$	306.0737	307.0838	M-H	70-18-8	HMDB0062697	C00051	143.0461;128.0352;99.0564
353	13-HpODE	$C_{18}H_{32}O_4$	311.2220	312.2301	M-H	23017-93-8	—	—	183.0117
354	Ethyl stearate	$C_{20}H_{40}O_2$	311.2950	312.3028	M-H	111-61-5	HMDB0034156	—	183.0117;283.8555
355	Acetylaspartylglutamic acid	$C_{11}H_{16}N_2O_8$	320.0880	304.0907	M+NH_4-2H	3106-85-2	HMDB0001067	C12270	115.0207;128.0351
356	Cytidine monophosphate	$C_9H_{14}N_3O_8P$	322.0409	323.0519	M-H	63-37-6	HMDB0000095	C00055	78.9591;96.9696
357	Uridine 5-Monophosphate	$C_9H_{13}N_2O_9P$	323.0290	324.0359	M-H	58-97-9	HMDB0000288	C00105	78.9591;96.9696;111.0199
358	Docosahexaenoic acid	$C_{22}H_{32}O_2$	327.2170	328.2402	M-H	25377-50-8	HMDB0002183	C06429	150.0171;181.0591

359	Fructose-2,6-diphosphate	$C_6H_{14}O_{12}P_2$	338.9890	339.9961	M-H	—	HMDB0001047	C00665	96.96
360	Quercetin	$C_{15}H_{10}O_7$	338.9890	302.0427	M+K-2H	117-39-5	HMDB0005794	C00389	283.8553;302.7115
361	Heneicosanoic acid	$C_{21}H_{42}O_2$	339.3260	326.3185	M-H	2363-71-5	HMDB0002345	—	283.8548
362	Penicillin v	$C_{16}H_{18}N_2O_5S$	371.0650	350.0936	M+Na-2H	1987/8/1	HMDB0014561	C08126	93.0344
363	Cysteine-glutathione disulfide	$C_{13}H_{22}N_4O_8S_2$	442.1120	426.0879	M+NH_4-2H	13081-14-6	—	C05526	381.4482;158.9249
364	5'-DGTP	$C_{10}H_{16}N_5O_{13}P_3$	505.9880	506.9957	M-H	2564-35-4	HMDB0001440	C00286	158.9254
365	UDP-D-galactose	$C_{15}H_{24}N_2O_{17}P_2$	565.0470	566.0550	M-H	2956-16-3	HMDB0000302	C00052	323.0275;384.9829;241.0111
366	UDP-glucose	$C_{15}H_{24}N_2O_{17}P_2$	565.0470	566.0550	M-H	—	HMDB0060079	—	323.0275;384.9828;241.0110
367	Uridine diphosphate glucuronic acid	$C_{15}H_{22}N_2O_{18}P_2$	579.0270	580.0343	M-H	2616-64-0	HMDB0000935	C00167	402.9937
368	UDP-N-acetylglucosamine	$C_{17}H_{27}N_3O_{17}P_2$	606.0750	607.0816	M-H	528-04-1	HMDB0000290	C00043	158.9251;272.9564;282.0376

5. References

[1] R. N. Li, Y. L. Shao, Y. M. Yu, X. Y. Wang, G. S. Guo, *Chem. Commun.* **2017**, *53*, 4104−4107.

[2] X. Y. Wang, Y. L. Shao, L. Wang, G. S. Guo, ZL201610125665.4, **2016**.

[3] R. H. Wang, H. S. Zhao, X. C. Zhang, X. Zhao, Z. Song, J. Ouyang, *Anal. Chem.* **2019**, *91*, 3667−3674.

[4] Z. W. Wei, S. Han, X. Y. Gong, Y. Y. Zhao, C. D. Yang, S. C. Zhang, X. R. Zhang, *Angew. Chem. Int. Ed.* 2013, 52, 11025 –11028.

[5] L. Rayleigh, *Philos. Mag.* **1882**, *14*, 184−186.